The Oxygen Production Pre-Combustion (OPPC) IGCC plant for efficient power production with CO_2 capture

*Carlos Arnaiz del Pozo[2], Schalk Cloete[1], Jan Hendrik Cloete[1], Ángel Jiménez Álvaro[2], Shahriar Amini[1]**

[1] SINTEF Industry, Trondheim, Norway

[2] Universidad Politécnica de Madrid, Madrid, Spain

*Corresponding author:

Shahriar Amini

S.P. Andersens vei 15B, 7031 Trondheim, Norway

+4746639721

shahriar.amini@sintef.no

Abstract

This work presents a novel integrated gasification combined cycle (IGCC) power plant configuration for CO_2 capture with minimal energy penalty. The proposed oxygen production pre-combustion (OPPC) power plant synergistically integrates a gas switching oxygen production (GSOP) unit into a pre-combustion IGCC power plant, reducing the energy penalty through two channels: 1) avoidance of a cryogenic air separation unit and 2) pre-heating the air sent to the combined power cycle, which reduces the steam requirement for shifting CO to H_2 and the CO_2 capture duty involved in pre-combustion CO_2 capture. Relative to a conventional pre-combustion IGCC benchmark, the OPPC configuration improves the electric efficiency by about 6 %-points, although the CO_2 capture ratio reduces by about 6 %-points. OPPC as avoids the maximum temperature limitation of Chemical Looping Combustion based plants, and can therefore benefit from efficient modern gas turbine technology operating at very high inlet temperatures. CO_2 removal via physical absorption (Selexol) generally results in higher efficiencies, but lower CO_2 avoidance than chemical absorption (MDEA). Plant efficiency also benefits from an increase in GSOP operating temperature, although the maximum temperature was limited to 900 °C to avoid any temperature-related challenges with oxygen carrier stability or downstream valves and filters. OPPC therefore appears to be a promising configuration for minimizing the energy penalty of CO_2 capture in IGCC power plants, combining well known and proven technology blocks with a GSOP reactor cluster instead of an ASU.

Keywords: Gas switching oxygen production, CO_2 capture, efficiency, integrated gasification combined cycle, pre-combustion.

List of symbols

Main symbols:

C_p	Heat capacity (J/kmol/K)
F	Molar flow rate (kmol/s)
ΔH_k^R	Reference enthalphy of reaction (J/kmol)
h	Enthalphy (J/mol)
N	Amount of species (kmol)
P	Pressure (Pa)
R	Reaction rate (kmol/s)
s	Stoichiometric coefficient
T	Temperature (K)
t	Time (s)
y	Mole fraction

Subscripts and superscripts:

g	Gas
i, j	Species index
k	Reaction index

s Solids

Acronyms:

ASU Air separation unit

CCS CO_2 capture and storage

CLC Chemical looping combustion

GSC Gas switching combustion

GSOP Gas switching oxygen production

HHV Higher heating value

HRSG Heat recovery steam generator

HGCU Hot gas clean-up

IGCC Integrated gasification combined cycle

IPPC Intergovernmental Panel on Climate Change

LHV Lower heating value

MDEA Methyldiethanolamine

SEC Syngas effluent cooler

SFT Stoichiometric Flame Temperature

TIT Turbine inlet temperature

TOT Turbine outlet temperature

WGS Water Gas Shift

1 Introduction

1.1 Outline & purpose of this work

The recently released IPCC special report on global warming of 1.5 °C [1] has reemphasized the urgency of reducing global greenhouse gas emissions. Power systems employing coal as fuel constitute the biggest source of environmental pollution [2] which lead to public health concerns and cause the greenhouse effect. Consequently, several EU countries have intensified their efforts to phase out coal by 2030 increasing the power share of renewable sources [3]. However, large scale substitution of coal with solar and wind presents substantial challenges to ensuring reliable supply, particularly when the availability of electricity does not match demand patterns [4]. Furthermore, developing countries with a coal-reliant energy structure such as China will not be able to eliminate its predominance in the short term [5].

CO_2 capture and storage (CCS) will play a central role in meeting the ambitious climate change targets: the IPCC fifth assessment report concluded that the total costs of decarbonization will increase by 140% for scenarios achieving atmospheric $CO_{2,eq}$ concentrations of 450 ppm by 2100 if CCS is eliminated as a technology option [6]. In fact, most model runs could not even achieve a feasible 450 ppm solution without CCS.

CCS is a technologically viable and a low-carbon development opportunity but, in order to fulfil its potential as a cost-effective solution for rapid decarbonization of the global economy, it is very important to reduce the energy penalty of CO_2 capture. Conventional CO_2 capture from coal-fired power plants requires about 30% greater fuel consumption per unit electricity output [7]. Aside from the increased fuel cost, the specific capital cost ($/kW) of the plant also increases because a larger plant is needed to produce a fixed electricity output. In addition, the greater fuel consumption increases the environmental impact related to fuel production and transport, eroding a significant portion of the environmental benefit of CCS [8]. The lower efficiency also increases the quantity of CO_2 produced per unit electricity, magnifying the challenge of CO_2 transport and storage.

Thus, a novel solid-fuel power plant concept with a low energy penalty for CO_2 capture is presented in this work. Special emphasis is placed on the technical feasibility of the solution by circumventing key technical challenges associated with other efficient CO_2 capture power plant configurations.

1.2 Inherent carbon capture strategies

One promising solution for reducing the energy penalty of CO_2 capture is chemical looping combustion (CLC) [9, 10]. CLC employs an oxygen carrier material to transport oxygen from an air reactor, where it is oxidized by air, to a fuel reactor, where this oxygen is used to combust a fuel in an N_2-free environment. In this way, CLC achieves oxyfuel CO_2 capture without the energy penalty related to an air separation unit.

Two main avenues of CLC are being pursued: solid-fuelled CLC and gas-fuelled CLC. Solid-fuelled CLC injects the solid fuel directly into the fuel reactor where it gasifies and reduces the oxygen carrier. This type of CLC can operate at atmospheric pressure and benefit from existing circulating fluidized bed solid fuel combustion technology [11], but also introduces a number of important challenges. The three most important challenges include syngas slip from fuel gasified in the upper regions of the bed, unreacted char that requires a dedicated carbon stripper unit to prevent it leaking to the air reactor, and the need for a very cheap oxygen carrier that can be economically deployed over short lifetimes due to exposure to contaminants or losses with ash removal [12, 13].

Gas-fuelled CLC avoids these challenges, but encounters new challenges from the need to operate at high pressures and temperatures for integration into a combined cycle power plant. Operation under pressurized conditions (typically about 20 bar) complicates reactor design and operation, which is part of the reason why a recent review [14] listed only one pressurized gas-fuelled CLC demonstration out of the 20 reviewed studies.

The maximum achievable temperature will be limited by the oxygen carrier material and reactor body to a level well below the turbine inlet temperatures (TIT) achievable by modern highly efficient gas turbines (~1600 °C). This can cause a large reduction in power plant efficiency. For example, [15] assumed a conservative CLC temperature of 900 °C, resulting in an efficiency of only 41.2% in a natural gas CLC plant, whereas other studies assuming maximum temperatures up to 1200 °C, typically return efficiencies above 50% [16-18] and above 40% for IGCC plants [19, 20]. Even with a CLC operating temperature of 1200 °C, the achieved efficiency is still well below that of an unabated plant, and this energy penalty will continue to increase as gas turbine technology pushes the envelope to even higher TIT (e.g., 1700 °C targeted by Ito, Tsukagoshi [21]).

1.3 The oxygen production pre-combustion (OPPC) concept

This study seeks to address the dual challenge of high pressure and high temperature operation required for competitive efficiencies. The pressurization challenge is addressed by employing the gas

switching technology [22, 23] where the oxygen carrier material is kept in a single bubbling fluidized bed reactor and alternately exposed to reducing and oxidizing gases. This simple standalone reactor will be much simpler to scale up and operate under pressurized conditions than the conventional interconnected circulating fluidized bed system.

The temperature challenge is addressed by employing pre-combustion CO_2 capture to produce an H_2 stream that can be combusted without the need for an oxygen carrier or a reactor that will limit the maximum achievable temperature. It is well-known that pre-combustion CO_2 capture also imposes a substantial energy penalty of about 9.5 %-points in integrated gasification combined cycle (IGCC) plants [23], but the novel configuration proposed in this study eliminates most of this energy penalty through a synergistic integration with chemical looping oxygen production (CLOP) as shown in Figure 1.

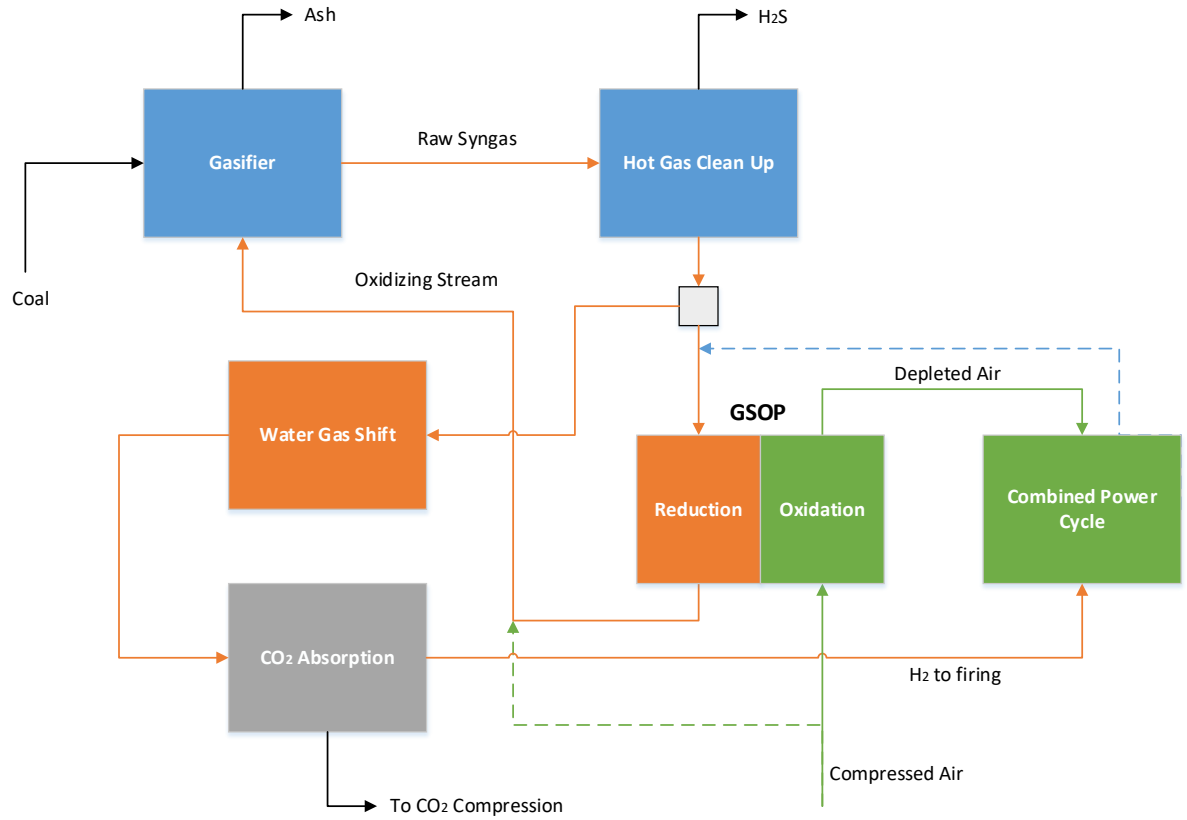

Figure 1: Simplified outline of the oxygen production pre-combustion (OPPC) IGCC plant proposed in this study. The dashed lines indicate two alternative methods for supplying enough oxygen to the gasifier: adding steam before GSOP or adding air after GSOP.

CLOP has been proposed as a more efficient solution relative to conventional cryogenic air separation units (ASU) [24] and has been modelled and optimized for its integration in an oxy-fuel combustion power plant [25]. As a standalone ASU, CLOP faces challenges with the requirements to heat the reducing reactor, recover heat from the high temperature depleted air stream, and carry out oxidation under significantly higher pressures than reduction to achieve good performance [26, 27].

However, in this work the CLOP reactor is integrated into an IGCC plant to circumvent these challenges. The reduction reactor can be efficiently heated by feeding carbonaceous fuel as part of the sweep gas, the hot depleted air stream can be efficiently utilized for power production in the combined cycle, and both reactor stages can be operated at similar and high pressure levels employing the gas switching concept. Such an integration was proposed by Cloete, Giuffrida [28] where the CLOP technology was

integrated with CLC in an IGCC plant, yielding an efficiency of more than 45%, about 2.3 %-points better than an IGCC plant with CLC only. The efficiency gain is mainly attributable to CLOP avoiding the energy penalty of an ASU. This combined CLOP-CLC-IGCC plant would be quite complex to operate and a subsequent economic assessment showed that it only achieved marginally better economics than the CLC-IGCC plant [29]. The use of the CLC reactors also puts a limit on the maximum achievable TIT, hampering the ability of the plant to capitalize on continued improvements in gas turbine technology.

The OPPC plant in Figure 1 replaces the CLC unit with a conventional pre-combustion train consisting of water-gas shift (WGS) reactors and a CO_2 capture unit. The CLOP system is operated in gas switching mode for easy scale-up and pressurization and is henceforth called gas switching oxygen production (GSOP). A significant fraction of the fuel is combusted in the GSOP reactors following the CLC mechanism to maintain the GSOP reactor temperature. This fuel is combusted with almost no energy penalty or CO_2 emissions. As a result, the pre-combustion train can be downsized to produce only enough H_2 to heat the depleted air stream from the GSOP operating temperature to the TIT. In addition, GSOP eliminates most of the energy penalty associated with a conventional ASU. Compared to the CLOP-CLC-IGCC plant proposed by Cloete, Giuffrida [28], the novel OPPC plant presented in this work yields the following benefits:

1. The ability to raise the TIT to the maximum that is achievable by state-of-the-art turbines.
2. Operation of GSOP at moderate temperatures, avoiding any temperature-related limitations of the oxygen carrier, reactor body or downstream valves and filters (which avoid solids carryover to the turbomachinery).
3. Removal of the two-way coupling between CLOP and CLC that will complicate plant operation and hamper flexibility.
4. No need for dedicated heat recovery from the hot CO_2-rich stream exiting the CLC unit.
5. Use of commercially available technology blocks for CO_2 sequestration (WGS and Absorption units).

Ultimately, the OPPC concept presents an innovative integration of the GSOP reactors in a pre-combustion train and power cycle, revealing substantial reductions in energy penalty relative to a conventional IGCC plant with pre-combustion CO_2 capture [30], eliminating energy intensive ASU's while overcoming the operational and material related challenges that CLC concepts present. Due to these fundamental advantages, this work will investigate the performance of the OPPC plant in detail, quantifying its efficiency and CO_2 capture rate relative to a conventional IGCC pre-combustion benchmark.

2 Reactor simulations

The transient behaviour of the GSOP reactors is simulated using a 0D model developed in Matlab R2018b. The model is based on two important assumptions: 1) that the fluidized beds that are employed can be assumed to behave like ideal CSTR reactors and 2) that thermal- and chemical equilibrium is reached in the reactors. The former assumption is reasonable considering the excellent mixing achieved in fluidized bed reactors, whereas both the thorough mixing and the large reactor geometries considered for industrial scale fluidized beds give validity to the latter.

2.1 Reactions

In the gas switching process, an oxygen carrier material is alternately oxidized and reduced by switching the inlet stream to the reactor. However, for the GSOP process, the oxygen carrier material should also have the ability to release free oxygen. For this purpose $Ca_2AlMnO_{5.5}$ is considered. This oxygen carrier was developed by Motohashi, Hirano [31] and investigated in an earlier modelling study

[28]. Many other potential oxygen carriers with the oxygen uncoupling capability exist. The classic materials are Cu-, Mn- and Co-oxides [24], but many other candidates exist [32] offering the potential to operate the process over a range of temperatures.

The oxygen carrier will participate in four heterogenous reactions in the GSOP process. In the first three reactions, the oxygen carrier is reduced by different fuels in the reduction stage. In the fourth reaction, the oxygen carrier releases oxygen in the reduction stage and is regenerated in the oxidation stage.

$$CH_4 + 8Ca_2AlMnO_{5.5} \rightarrow 8Ca_2AlMnO_5 + CO_2 + 2H_2O \qquad R_1 = \frac{1}{\tau} N_{CH_4} N_{Ca_2AlMnO_{5.5}} \qquad \text{Eq. 1}$$

$$H_2 + 2Ca_2AlMnO_{5.5} \rightarrow 2Ca_2AlMnO_5 + H_2O \qquad R_2 = \frac{1}{\tau} N_{H_2} N_{Ca_2AlMnO_{5.5}} \qquad \text{Eq. 2}$$

$$CO + 2Ca_2AlMnO_{5.5} \rightarrow 2Ca_2AlMnO_5 + CO_2 \qquad R_3 = \frac{1}{\tau} N_{CO} N_{Ca_2AlMnO_{5.5}} \qquad \text{Eq. 3}$$

$$O_2 + 4Ca_2AlMnO_5 \leftrightarrow 4Ca_2AlMnO_{5.5} \qquad R_4 = \frac{1}{\tau}\left(y_{O_2} - y_{O_2,eq}\right) \times N_{\text{gas}} N_{Ca_2AlMnO_{5.5}} \qquad \text{Eq. 4}$$

In the above reactions, N_i denotes the amount of species i (in kmol) present in the reactor and y_i the mole fraction of species i. The value of τ is set to 0.01, which ensures that the reaction rates (R_1, R_2, R_3, R_4) are always fast enough that the reactions proceed to equilibrium. From a previous study [28], the equilibrium oxygen mole fraction was determined as:

$$y_{O_2,eq} = \frac{1}{P} \exp\left(-\frac{91000}{R}\left(\frac{1}{T} - \frac{1}{T_{ref}}\right)\right) \qquad \text{Eq. 5}$$

A value of 720 °C for T_{ref}, determined from TGA experiments, was used in the aforementioned study [28]. Since GSOP oxygen carriers are still in an early stage of development and many potential candidate materials are available, the present study also included a sensitivity analysis to the temperature in the GSOP reactors. The optimal reactor temperature is primarily dependent on the properties of the oxygen carrier when considering a constant pressure. This study therefore varied the value of T_{ref} in Eq. 5 over the three levels indicated in Table 1 to achieve optimal GSOP reactor operation at three different average reactor temperatures. The required values of T_{ref} changed slightly between the two methods for supplying enough oxygen to the gasifier (Figure 1). This requirement to modify T_{ref} for achieving different reactor operating temperatures arises from the equilibrium nature of the oxidation reaction (Eq. 4). For example, if T_{ref} is kept constant and an attempt is made to increase the reactor temperature, the equilibrium in Eq. 4 will shift to the reactant side and it will no longer be possible to achieve sufficient oxidation of the oxygen carrier. In practice, different oxygen carrier materials will need to be selected to enable operation of the GSOP reactors at different temperatures.

Table 1: Three levels of T_{ref} in Eq. 5 assumed to achieve the three different average GSOP operating temperatures investigated in this study in the Air to Gasifier and Steam to GSOP cases.

Reactor temperature	T_{ref} in Eq. 5	
	Air to Gasifier	Steam to GSOP
700 °C	604 °C	609 °C
800 °C	690 °C	694 °C

900 °C	776 °C	779 °C

2.2 Mole and energy balances

The following conservation equations are solved in the 0D model using Matlab's ode15 differential-algebraic equation solver and are described here briefly.

$$\frac{dN_{g,i}}{dt} = F_g^{in} y_{g,i}^{in} - F_g y_{g,i} + \sum_k s_{i,k} R_k \quad \text{Eq. 6}$$

$$\frac{dN_{s,j}}{dt} = \sum_k s_{j,k} R_k \quad \text{Eq. 7}$$

$$\left(\sum_i N_{g,i} C_{Pi} + \sum_j N_{s,j} C_{Pj} \right) \frac{dT}{dt} = \sum_i \left(F_g^{in} y_{g,i}^{in} h_{g,i}^{in} - F_g y_{g,i} h_{g,i} \right) + \sum_k R_k \Delta H_k^R \quad \text{Eq. 8}$$

Eq. 6 and Eq. 7 show the species conservation equations for the gas and solids phases, respectively. For Eq. 6, the respective terms from left to right represent the rate of change of the total moles, the molar flow into the reactor, the molar flow out of the reactor and the change in moles due to chemical reactions. For the solid phase conservation equation, no inflow or outflow of solids is present. Finally, Eq. 8 solves the enthalpy conservation equation for the system. From left to right, the terms represent the rate of change of enthalpy, the flow of enthalpy into the reactor, the flow of enthalpy out of the reactor and the enthalpy change through reactions.

2.3 Boundary, material and operating conditions

The flow rates, compositions, temperatures and pressures of the inlet gas streams are obtained from the process simulations. A cylindrical reactor with a height of 12 m and a diameter of 7 m is chosen. This will result in a fluidization velocity of around 0.3 m/s in the GSOP reactor, which will yield bubbling fluidization conditions when using a typical particle size of around 150 µm. The reactor sizing will become more important in future economic assessments of the OPPC concept where an optimum between lower capital costs of small reactors and higher reactant conversion of large reactors must be found. A density of 3000 kg/m^3 is assumed for the solids, which is a typical value for fluidized bed applications, as well as an average volume fraction of 0.35 in the reactor. Furthermore, according to an earlier study [28], the oxygen carrier is specified to contain 75% by mass of active material, with the rest being inert.

In the 0D simulations, the total amount of fuel fed to the reduction stage and the relative inlet flow rates in the reduction and oxidation stages were dynamically tuned to ensure that the oxygen carrier cycles between 10% and 90% oxidation by weight of the active material. This ensures that the reaction rates in Eq. 1 to Eq. 4 will not slow down drastically when the oxygen carrier is close to either complete oxidation or reduction, which would invalidate the assumption that chemical equilibrium is always reached. Furthermore, the relative stage lengths of the reduction and oxidation stages were chosen as the integer value that yielded the most similar molar outlet flow rates of the two stages. This was done to allow the use of a delayed outlet switch, which significantly reduces the amount of undesired mixing between the stages [23]. It can be noted that for a reduction/oxidation stage time ratio of $1/x$, a cluster of $x + 1$ reactors would be required, with 1 reactor operating in the reduction stage and x reactors operating in the oxidation stage at any moment in time.

2.4 Link to the process model

Inlet boundary conditions for the reactor simulations were obtained from the process simulations. The reactor simulations were then performed to determine values for the average temperatures and oxygen mole fractions of the reduction and oxidation stage outlet streams, as well as the fraction of mixing between the stages. These values were then updated in the process simulations to predict a new set of boundary conditions to the reactor. These steps were repeated until a converged solution was achieved.

2.5 Reactor Simulation results

To describe the reactor behaviour for the GSOP process, Figure 2 shows the reactor outlet temperature and compositions over a full reactor cycle for six different cases. In all cases, it can be seen that, during the fuel stage, the fuel is combusted to H_2O and CO_2 by oxygen from the oxygen carrier, also releasing heat which increases the outlet temperature. Additionally, the oxygen carrier releases oxygen which can be used in the gasifier. In the subsequent oxidation stage, the oxygen carrier is regenerated by air. Despite this reaction being exothermic (ΔH = -91 kJ/mol), the reactor temperature decreases due to the large amount of air that must be heated up and the relatively small fraction of the oxygen in air that reacts with the oxygen carrier.

At the start of the oxidation stage, the undesired mixing of CO_2 into the oxidation stage products, which will reduce the carbon capture efficiency, can be observed. Furthermore, it can be seen that the oxygen mole fraction in the reactor outlet follows the trends of the reactor temperature due to the equilibrium reaction between the oxygen carrier and oxygen. Due to the non-linear trend of the temperature in the oxidation stage, the average oxygen mole fraction in the oxidation stage will tend to be lower than that in the reduction stage. This difference will be greater for cases with relatively more air being added (longer dimensionless cycle time when scaled by the fuel stage time) since the temperature profile flattens out more during the longer air stages.

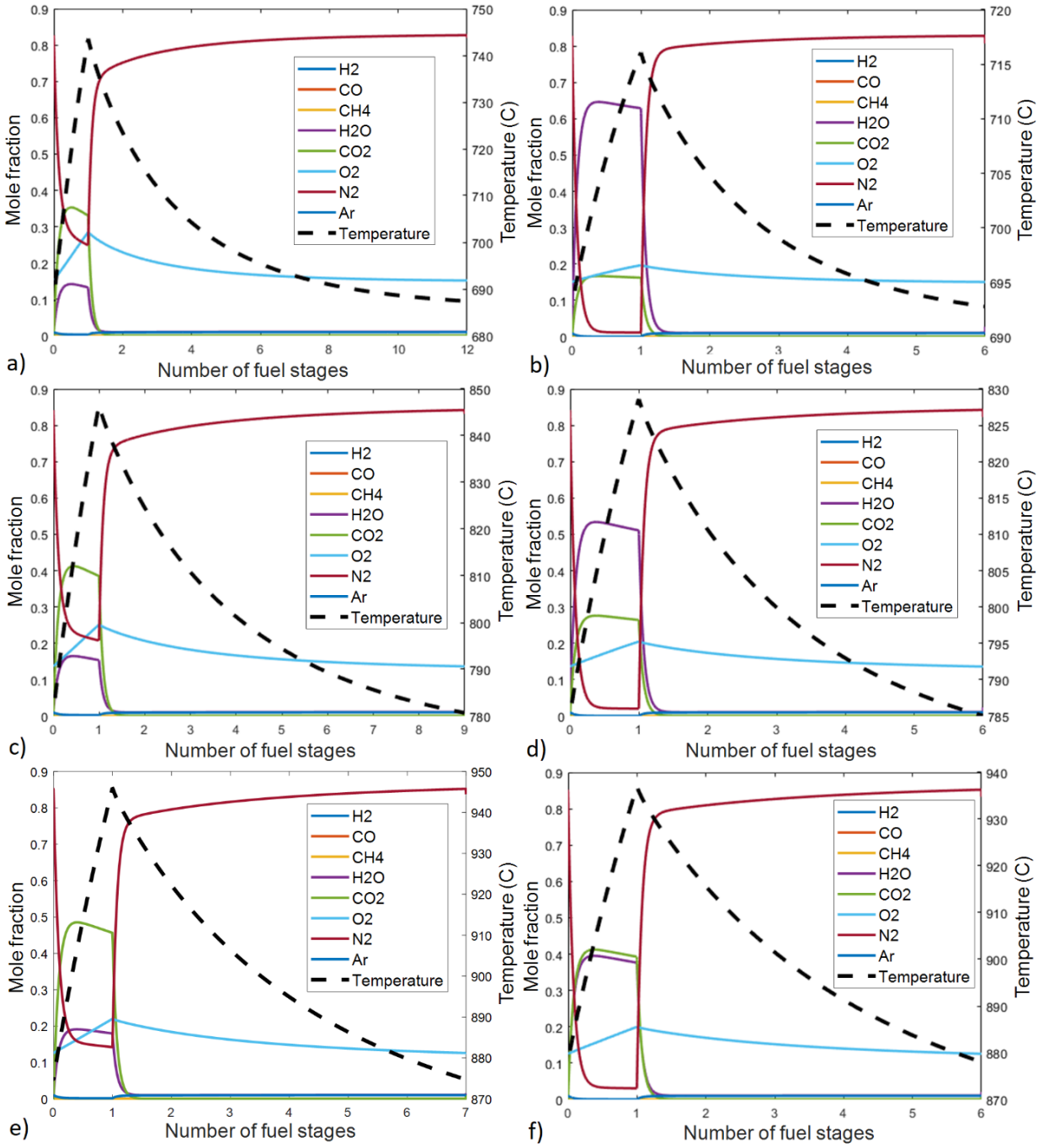

Figure 2: Temperature and compositions at the reactor outlet during a full cycle for different reactor simulations. The left column shows Air to Gasifier cases and the right column Steam to GSOP. From top to bottom the rows show cases with average oxidation stage temperatures of 700°C, 800°C and 900°C

As described in Figure 1, two ways were explored to supply enough O_2 to the gasifier: 1) feeding additional steam to the GSOP reduction stage inlet to increase the amount of sweep gas and enable more extraction of free O_2 from the oxygen carrier (henceforward Steam to GSOP cases) and 2) adding air to the GSOP reduction stage outlet to directly increase the oxygen flowrate in the stream to the gasifier (henceforward Air to Gasifier cases).

The primary difference between the case with Air to the gasifier (left-hand column in Figure 2) and the case with Steam to the GSOP (right-hand column in Figure 2) is the composition of the reduction stage outlet stream, which is diluted by nitrogen in the Air to Gasifier cases and by steam in the Steam to

GSOP cases. For the Air to Gasifier cases, the length of the oxidation stage decreases substantially with increasing reactor temperature. This is because, at higher reactor temperatures, the incoming air stream must be heated to a higher temperature and therefore less air is required to remove the combustion heat from the reactor.

For the Steam to GSOP cases, relatively less air is required for all the cases considered. This is because the steam addition reduces the heating value of the inlet syngas stream to the reduction stage, thereby requiring relatively less air to remove the reaction heat from the reactor. Also, the heating value tends to increase with increasing reactor temperature since relatively less steam is required to dilute the syngas, thereby offsetting the effect of the reactor temperature on the amount of air required, as observed in the Air to Gasifier cases. Less steam addition is required in the higher temperature cases for two reasons: 1) a larger portion of the syngas from the gasifier must be diverted to the GSOP to heat the air to a higher temperature and 2) the gasifier oxygen demand reduces with increasing temperature of the oxidant stream fed to the gasifier.

3 Power Plant Description

The power plant configurations presented in this work were modelled with UniSim Design R451 from Honeywell using Peng-Robinson equation of state to predict thermodynamic properties of the streams. The steam cycle was modelled using ASME Steam tables, while the Henry coefficients of different components in Selexol were taken from Kapetaki, Brandani [33]. Lastly, MDEA absorption was simulated with the DRB amine property package available in UniSim thermodynamic database. UniSim allows an integrated model of the different sections of the plant, representing gas switching technology with time averaged operating temperatures and flow rates.

3.1 IGCC with Pre-combustion Capture

The integrated gasification combined cycle (IGCC) presented as benchmark in this work is depicted in Figure 3. In this configuration, extensively studied in previous works [30], gasification of coal takes place in a Shell gasifier with oxygen provided from an Air Separation Unit (ASU). After particulate removal and steam addition, a shift reaction section converts CO to H_2. CO_2 and H_2S are selectively removed in a Selexol absorption unit. After dilution with N_2 and water saturation, the hydrogen stream is fired in a gas turbine. The exhaust heat is transformed to extra power by means of a heat steam recovery generator with three pressure levels and intermediate pressure reheat. The following sections give a more detailed description of the elements of the pre-combustion capture power plant.

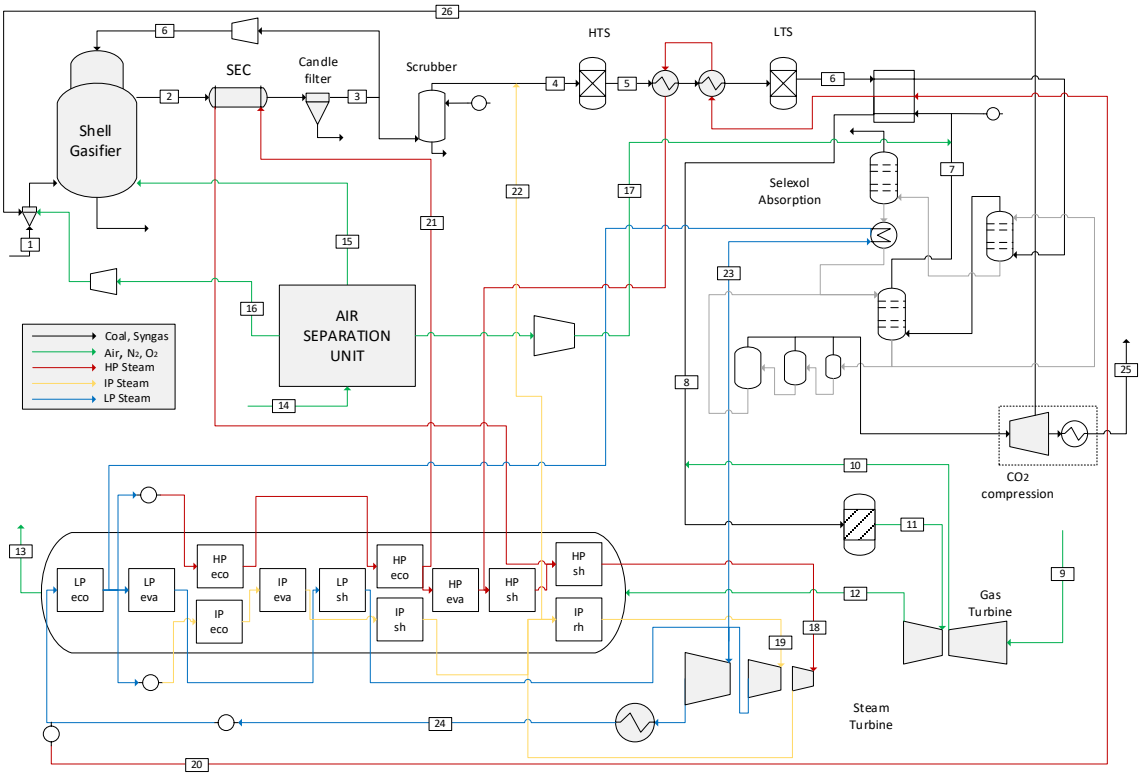

Figure 3 Power plant diagram of the precombustion capture IGCC model in Unisim. Stream data can be found in the Appendix

3.1.1 Gasification Island

Dry Douglas Premium Sub-bituminous coal (2% moisture content) is gasified in an entrained flow gasifier, Shell type, with 95% mol purity O_2 provided by a standalone (non-integrated for availability reasons) reboiler-condenser ASU. The ASU uses a cryogenic pump to deliver O_2 at the required pressure to the gasifier (48 bar), while high purity nitrogen (>99%) is delivered partly at an intermediate pressure (5.5 bar) and the major portion of the flow at 1.2 bar. Nitrogen is further compressed and used for fuel dilution in the power island. The use of a cryogenic pump avoids an intercooled oxygen compressor, a costly element and critical equipment from a safety viewpoint, at the cost of a slightly higher power consumption. Pumped liquid oxygen cycles are usually preferred when the gasifier operates at a high pressure [34]. Coal is loaded primarily with CO_2 from the capture and compression section and with a small amount of N_2 provided by the ASU. The high operating pressure of the gasifier demands a substantial amount of inert gases for coal loading. It is assumed that 10% of the mass flow rate of CO_2 is vented in the lock hoppers, while 60% is retrieved and recompressed for capture. The remaining fraction enters the gasifier.

Gasification takes place at high temperatures and it is assumed that equilibrium composition is achieved. Solidified ash leaves the bottom of the gasifier, reaching a carbon conversion of 99.3%. The hot syngas is quenched with cold recycle syngas and leaves the gasifier at a temperature of 900 °C. A syngas effluent cooler (SEC) lowers its temperature further to 300 °C by raising HP steam. The SEC provides some steam superheat (450 °C) and acts as evaporator and economizer of HP water. Subsequently, the syngas goes through a ceramic filter that removes solidified entrained fly ash material, and is partly recompressed and quenched, while the remaining fraction is routed to a water scrubber that finally eliminates remaining particulate material and soluble contaminants. Gasification

island assumptions are similar to Spallina, Romano [35] and a detailed description of the modelling parameters can be found in in the Table 3 in the Appendix.

3.1.2 Water Gas Shift Section

The clean syngas is routed to a sour water gas shift unit which, after a substantial IP steam addition from HP stage outlet of the steam turbine, converts carbon monoxide with water to carbon dioxide and hydrogen as shown:

$$H_2O + CO \rightarrow H_2 + CO_2 \quad \Delta H^{\circ} = -41.15\ kJ/mol \qquad \text{Eq. 9}$$

The water gas shift reaction is mildly exothermic, and indifferent to pressure (the number of moles does not change). There is a substantial flexibility on operating temperatures for WGS catalysts, but lower temperatures increase the equilibrium conversion because of its exothermic nature. A relevant advantage of the sour WGS catalysts typically used in IGCC applications is that they are able to convert organic sulphur compounds to hydrogen sulphide, avoiding an intermediate hydrolyser and cooling-reheating of the syngas.

The reaction takes place in two steps with intercooling, to increase overall conversion. More optimal configurations for IGCC applications have been proposed in the past [36, 37], but in this work a standard layout based on the work of Franco, Anantharaman [38] is presented. In the first packed bed, at an inlet temperature of approximately 260 °C, the bulk conversion takes place. A steam to CO ratio of 1.9 was fixed to prevent methanation and carbon formation by limiting the adiabatic temperature rise to 507 °C [39]. High steam to CO ratios increase conversion but impact the steam cycle performance negatively, so optimization of this system aims to reduce the steam consumption. The heat released in the first reactor is downgraded to HP steam produced in an economizer and evaporator. The effluent is cooled to 200 °C and enters the second low temperature shift reactor reaching an overall conversion of approximately 98%. The temperature rise in the second reactor is much smaller (247 °C at the outlet). The shifted syngas is cooled down in a multistream heat exchanger which acts as water economizer and water heater for syngas saturation. After cooling to 25 °C and removing condensed water, the syngas is routed to the CO_2 removal unit. Detailed description of the modelling assumptions taken in for the simulation are shown in Table 6 in the Appendix.

3.1.3 CO_2 Absorption Unit

The CO_2 absorption unit is a selective H_2S and CO_2 separation unit consisting of two absorption columns with Selexol as a solvent, an H_2S concentrator, an H_2S stripper and a series of flash vessels where the solvent is regenerated. Selexol is a physical solvent which is particularly favoured for IGCC applications employing Shell gasification, because the partial pressure of CO_2 is high and the duty requirements for solvent regeneration (only the H_2S stripper) are substantially lower than for amine chemical solvents. The regeneration of CO_2 rich solvent does not require any thermal input and is performed in a series of consecutive flash vessels with decreasing pressure. Since purified CO_2 is obtained at higher pressures, the compression requirements are also lower than when a chemical solvent such as MDEA (with a stripper operating at near atmospheric pressure) is used.

The process topology for this section is similar to the one presented in Kapetaki, Brandani [33]. To accurately model the properties of Selexol, the Henry coefficients presented in the aforementioned study were employed. The mechanical work required for solvent recirculation and the thermal duty for H_2S stripping with LP steam were determined. The H_2S concentrator was modelled in such a way as to achieve an H_2S concentration of approximately 30% mol in the stream routed to the Claus unit (the tail gas is recycled to the absorption stage). The H_2S recovery was above 99.9% while the fraction of this contaminant in the compressed CO_2 stream was below 20 ppm. Further details of the modelling assumptions of this section can be found in Table 8 in the Appendix.

3.1.4 CO_2 compression

The CO_2 delivered by the Selexol process is compressed to 150 bar by means of a five stage CO_2 compressor with interstage cooling and a supercritical CO_2 pump. The high purity achieved after absorption prevents the need of any purification system. Knock out drums after the last three stages remove condensed water reaching a final purity above 99%mol. Modelling assumptions are detailed in Table 9 in the Appendix.

3.1.5 Power Island

The hydrogen-rich syngas delivered by the absorption step is mixed with hot nitrogen provided by the ASU and saturated with water. Before dilution, a small portion is withdrawn for coal drying. Heat is provided by residual thermal duty from the WGS section and subsequently further heated to 200°C before being fired in the gas turbine combustor with compressed air. Nitrogen available from the ASU is compressed in an intercooled compressor resulting in a significant auxiliary power consumption.

The criteria adopted to prevent NOx formation was to reach a stoichiometric flame temperature (SFT) of 2200 K, a reasonable value as shown in the work of Chiesa, Lozza [40]. The SFT was calculated by reacting the available syngas flow rate with a stoichiometric amount of air at the conditions of the compressor outlet. Despite the high temperatures of this model, it was assumed that the specific heat capacities of the substances involved were correctly estimated with Peng Robinson equation of state. SFT approach to determine dilution requirements is the most adequate measure (compared to fixing syngas LHV or the H_2/Inert ratio) as it takes into account the different heat capacities of N_2 and steam as dilution agents and because different air inlet temperatures to the combustion chamber are considered in these models.

The power plant size is determined by fixing a certain coal flow rate to the gasifier, with net power ranging from 320-380 MW. The steam cycle is a triple pressure cycle with intermediate reheat. The large demand for HP water of the SECs and the WGS heat recovery network leads to a minimal production of low pressure steam. The intermediate pressure level (40 bar) was set to match the pressure at the shift reactor inlet. The low pressure level (6.5 bar) was chosen to allow a reasonable approach in the H_2S stripper reboiler. For the high pressure level a value of 144 bar was adopted. Steam superheat was limited to 565 °C (in the HRSG) and to 450 °C in the syngas effluent cooler. Detailed process design parameters of these units are given Table 11 in the Appendix.

3.2 Oxygen Production Pre-Combustion (OPPC) IGCC Plant

The gas switching oxygen production integration with IGCC was proposed by Cloete, Giuffrida [28], where a complex configuration including GSOP and GSC reactor clusters is developed. The Oxygen Production Pre-Combustion OPPC plant eliminates the GSC, and replaces it with a shift conversion of a portion of the syngas. The aim is to produce hydrogen which can be combusted in the gas turbine in a carbon free environment, overcoming the limitations on TIT that oxygen metal carriers present (1200 °C) and boosting the TIT to a value of 1360 °C. With increasing TIT, the OPPC configuration would become even more attractive from an efficiency point of view.

The drawback is that a CO_2 capture absorption technology must be used after the shift (the CO_2 stream is not attained at a high pressure, increasing recompression efforts) and that a hot gas clean-up stage is required to eliminate H_2S before syngas enters the GSOP reactor. However, an important advantage of the OPPC concept is that high temperature valves and filters operating at temperatures close to 1200 °C, which is a potential showstopper for GSC configurations, are no longer needed (in the present study, GSOP operates at 900 °C as the highest temperature case, corresponding to the currently available filter technology limitations [41]). Additionally, the costly heat recovery unit of the reduction gases stream from GSC is removed, since the turbine outlet temperature (TOT) is substantially higher

and superheating of steam can be achieved efficiently in the exhaust gas HRSG as done in the pre-combustion IGCC plant. From an operational perspective, the power plant will be simplified substantially, as a technologically immature and challenging element is removed. An overview of this scheme is presented in Figure 4, where MDEA is used as CO_2 capture technology. The following sections describe in detail the different plant elements of the OPPC concept.

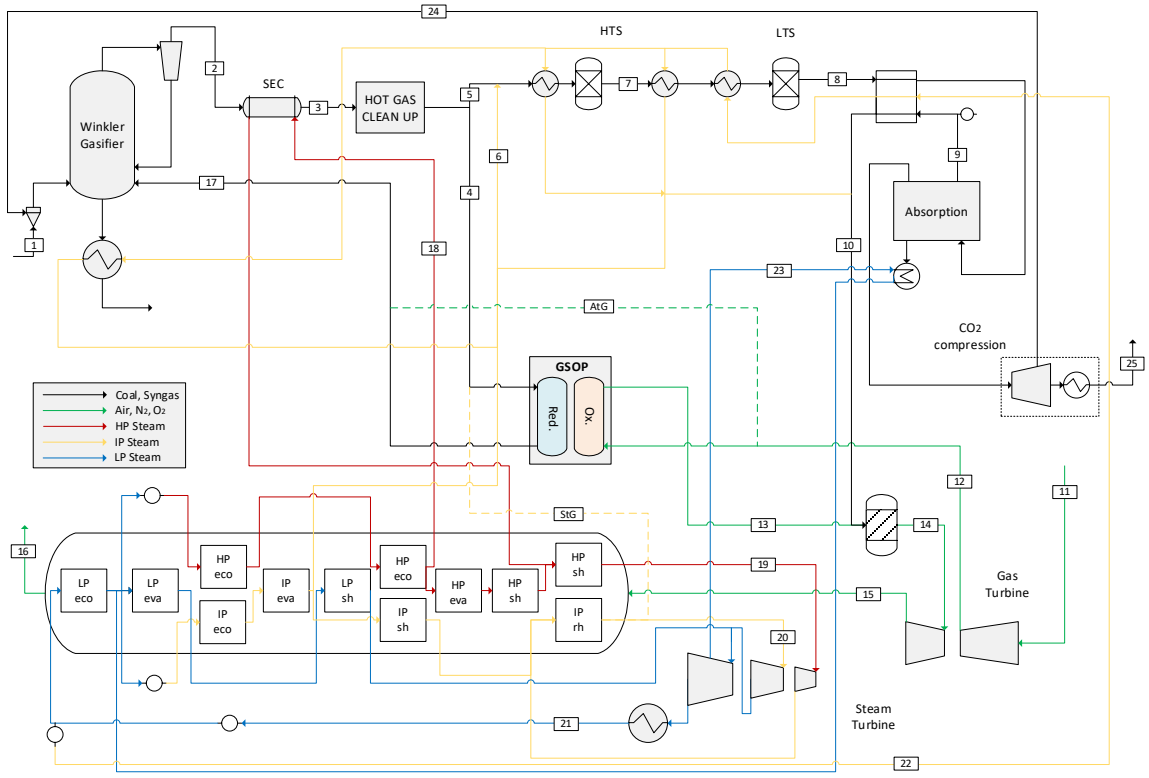

Figure 4: Simplified power plant diagram of the OPPC concept. Stream data is available in the Appendix.

3.1.6 Gasification Island

In the OPPC power plant, the oxidizing stream delivered by the GSOP has a low purity compared to that employed in the pre-combustion IGCC model. A fluidized bed, namely a High Temperature Winkler gasifier [28] proven for IGCC scale, delivers syngas at a temperature of around 900 °C. The gasifier produces no tars or liquid hydrocarbons and operates below the ash softening point, avoiding bed defluidization [42]. The good mixing properties of the fluidized bed allow a moderate temperature throughout it and long particle residence times avoiding excessive coal oxidation that would result from operation at higher temperatures in entrained flow gasifiers.

The gasifier operating pressure (19 bar) is slightly below the pressure ratio of the gas turbine, so the amount of CO_2 required for coal loading is significantly less than for the high pressure entrained flow gasifier. A fixed carbon conversion of 97% was assumed from Higman and van der Burgt [43]. A cyclone returns all solid material entrained with the syngas to the bottom of the gasifier to maximize overall conversion. To represent the lack of equilibrium conditions in the gasifier outlet, it was assumed that a fraction of methane corresponding to 11.3% of the coal LHV input is present in the syngas as done in Cloete, Giuffrida [28] for all cases. For future development, the gasifier model should be calibrated with real plant data to accurately determine syngas compositions for different oxidizing streams. The ash leaving the bottom of the gasifier is cooled in a radiant heat exchanger that generates IP steam used in the WGS section of the plant. Further modelling assumptions are detailed in Table 4 in the Appendix.

3.1.7 Syngas Treating

The syngas effluent cooler decreases the syngas temperature to 400 °C, generating HP steam with a certain degree of superheat (limited to 450 °C), followed by a dry filter which removes all entrained solid material before the syngas enters a hot gas clean up desulphurization unit. A Hot Gas Clean–Up (HGCU) unit was chosen to remove H_2S from the syngas stream to avoid the presence of this component in the GSOP reactors. The advantage of a high temperature sulphur removal unit is that syngas cooling and reheating is avoided before the WGS section and GSOP stages. The HGCU consists of a zinc oxide adsorption-regenerator interconnected fluidized bed where the following chemical reactions take place:

In the adsorption bed: $ZnO + H_2S \rightarrow ZnS + H_2O$: Eq. 10

In the regeneration bed: $ZnS + \frac{3}{2} O_2 \rightarrow ZnO + SO_2$ Eq. 11

Syngas after clean-up is filtered to avoid any adsorbent particulate material from entering the downstream units. Since no scrubber is present in this configuration, it is assumed that other sorbents are used to remove trace contaminants (HCN, HCl, NH_3 etc.) as described in Ohtsuka, Tsubouchi [44]. After the regenerative desorption stage, the stream containing SO_2 is routed to a wet scrubber where a sulphur recovery of 99% is achieved. The scrubber gaseous outlet is partly recirculated to the regeneration inlet, diluting the oxidising stream (air) and preventing undesired zinc sulphate formation. Further details of this syngas treating system are given in [28]. Since solvent regeneration and subsequent scrubbing units have a relatively low impact on plant efficiency, these steps were not modelled in the present work, but rather an auxiliary consumption factor was taken into account. A reasonable value for pressure drop and other process modelling assumptions of this unit are detailed in Table 5 in the Appendix.

3.1.8 Gas Switching Oxygen Production (GSOP)

The GSOP reactor cluster takes a portion of the desulphurized syngas as sweep gas in the reduction stage after a recompression blower which compensates the pressure losses. Combustion of H_2 and CO present in the syngas, as well as the release of free oxygen from the carrier take place, providing an oxidizing stream to the gasifier. The oxygen is removed from the compressed air stream from the gas turbine in the GSOP oxidation stage. In order to close the gasifier energy balance, either superheated intermediate pressure steam from the steam cycle (yellow dotted line in Figure 4, henceforward *Steam to GSOP* cases) or alternatively a small fraction of air from the gas turbine compressor (green dotted line in Figure 4, henceforward *Air to Gasifier* cases) is added to the GSOP sweep gas or GSOP reduction outlet respectively. Depending on the choice to close this balance, the resulting syngas has different composition, which has relevant implications on the size of the subsequent water gas shift section and absorption units. When air is sent to the gasifier, the resulting syngas is significantly diluted with N_2, whereas if steam is added as sweep gas in the GSOP, the H_2/CO ratio of the resulting syngas increases.

The effect of employing the GSOP to produce an oxidizing stream has the advantage of eliminating a costly and energy demanding ASU, with the side effect of preheating the compressed air stream (which will be subsequently sent to a combustion chamber) to GSOP oxidation temperature (700-900 °C). The fluidized bed operation causes a relevant pressure drop of the gaseous streams that was accounted for as 4% for all cases. Figure 5 shows the block flow diagram of the GSOP model in Unisim: time averaged values for operating temperatures of the two stages and mixing fractions of the gaseous streams are specified and given by the Matlab reactor model. Additionally, the O_2 production equilibrium was represented by fixing a certain value of the averaged O_2 concentration difference

between oxidation and reduction stage outlet streams based on the output of the Matlab reactor model.

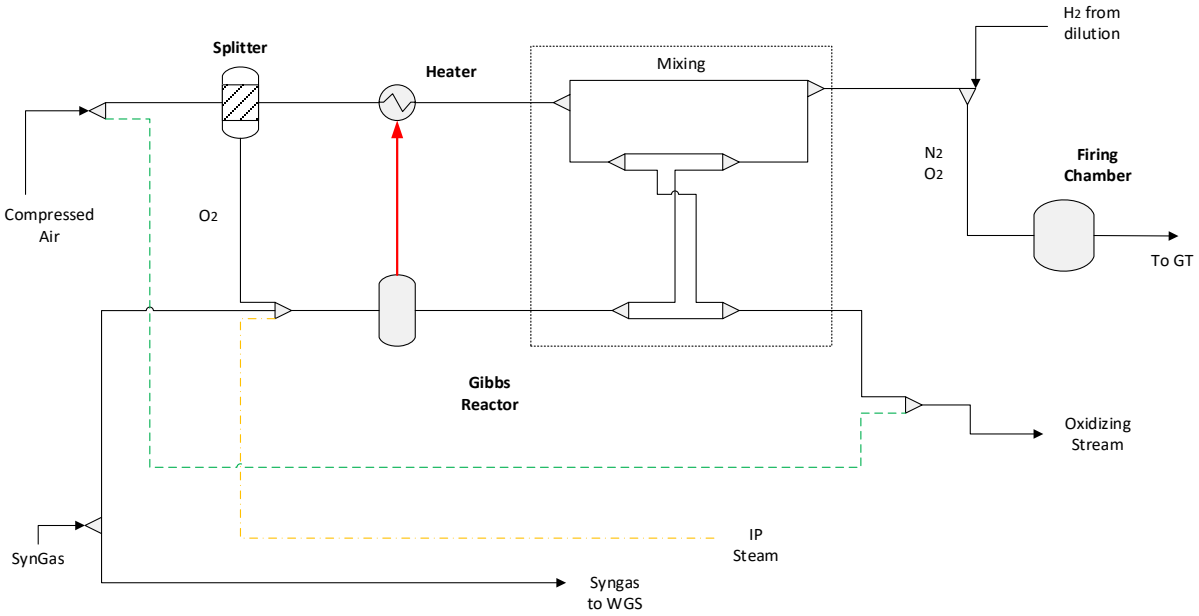

Figure 5 Process flow diagram of GSOP and firing chamber stationary model in Unisim.

Modelling assumptions for this section are given in Table 7 in the Appendix.

3.1.9 Water Gas Shift Section

The portion of syngas that is not routed to GSOP is shifted to generate a rich hydrogen stream which can be fired with GSOP oxidation outlet gases after dilution. The water gas shift layout in OPPC is identical to the pre-combustion plant, with the exception that, since no N_2 is available, steam for dilution is raised by heating more water in this section. Additionally, the syngas inlet has a relatively high fraction of inerts which leads to a reduction in the adiabatic temperature rise of the HTS reactor bed and thus, only IP steam is generated in the heat recovery units. The CO conversion is somewhat higher for the Air to Gasifier case, close to 99%, because of the presence of N_2 (which absorbs the heat of reaction increasing the equilibrium conversion), whereas the Steam to GSOP case reaches a CO conversion value slightly above 97% (a substantial amount of CO_2 product is already present). The steam to CO ratio was fixed to the same value as the pre-combustion model. It was assumed that the overall pressure drop across the WGS section was 1.8 bar.

3.1.10 Absorption Section

The shifted syngas is further cooled to 25 °C, removing condensed water, and sent to an absorption unit. The partial pressure of CO_2 is substantially lower than in the pre-combustion model because of the lower operating pressure of the gasifier (particularly lower in the Air to gasifier cases). Therefore, simulations with a chemical absorption system (MDEA 50%w) were performed. In order to show the trade-off between efficiency and capture rate, cases with Selexol were also run for different GSOP operating temperatures.

The process configurations employed are depicted in Figure 6, were only an absorber is used for the Selexol cases as opposed to the dual configuration in the pre-combustion model, since H_2S is no longer present in the syngas stream. The Unisim model determines the mechanical duty (solvent pumping, syngas recompression) and thermal demand for amine regeneration per kg of absorbed CO_2, reaching values which are in line with previous assessments [45, 46], with a somewhat lower mechanical power demand (which is reasonable because of the lower operating pressure of the absorbers). For all cases,

the amine process is configured to achieve a 95% removal of CO_2 from the syngas stream. Amine regeneration is performed with LP steam extraction from the steam turbine at 1.8 bar, while the amine stripper reboiler operates at 1.25 bar, slightly above atmospheric pressure to ease the CO_2 compression requirements. Selexol regeneration takes place in three flash vessels whose pressures were selected to minimize CO_2 compression. Further modelling assumptions of the amine system are detailed in Table 8 in the Appendix.

CO_2 solubility in Selexol is strongly dependent on its partial pressure. Therefore, given a number of equilibrium stages, the CO_2 recovery will be limited despite a large increase of the Selexol flow rate due to a pinch of the equilibrium and operating lines at the top of the absorber. In order to fix this value, it was adopted that, for all cases, 95% of the methane (with a relative solubility of 1/10 with respect to CO_2) remained in the syngas. This is a reasonable assumption since very high solvent flow will not significantly increase the capture rate and will have the drawback of entraining this component (with high heating value that improves the plant electric efficiency) alongside increasing the recirculation pump duty.

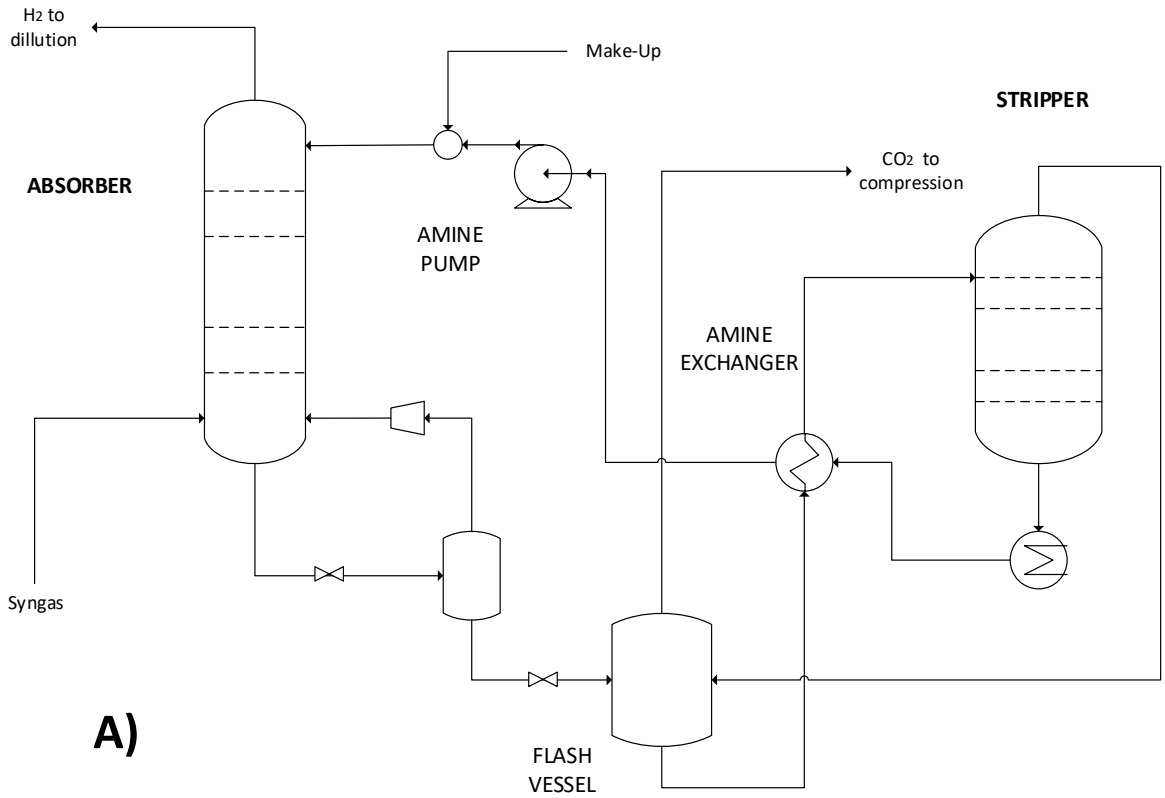

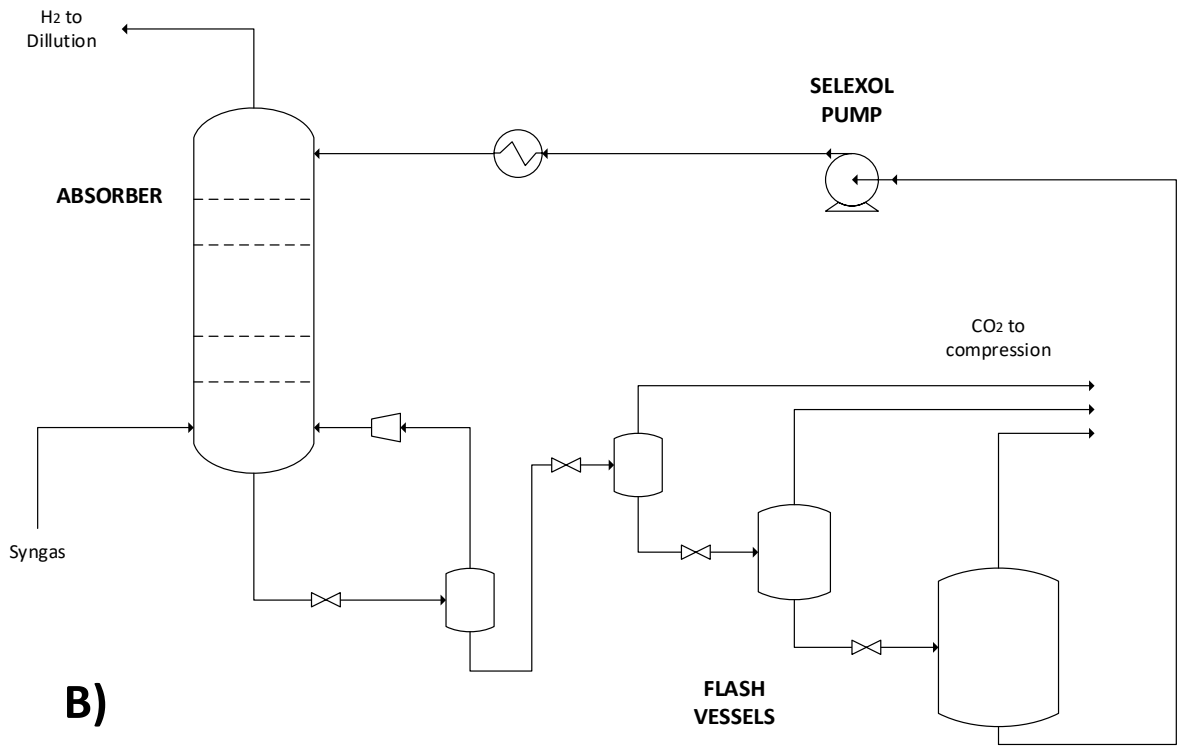

Figure 6: Process flow diagram of the A) chemical (MDEA) and B) physical (Selexol) absorption technologies investigated.

3.1.11 Power Island

The CO_2 stream from the absorption unit is compressed in an identical way as described for the pre-combustion model. H_2 is compressed and saturated with water. Steam is generated in the WGS section to satisfy the dilution requirements, since no nitrogen is available. A stoichiometric flame temperature of 2200 K was taken as a basis in the same way as for the pre-combustion model. The addition of water is minimal for the Air to gasifier cases since the syngas is already diluted with some N_2. Diluted fuel enters the combustion chamber at a temperature of 180 °C for all cases. This value is sufficiently above the dew point to avoid any liquid droplets in the combustor. The Gas Turbine, HRSG and Steam Turbine units are identical to the ones described for the pre-combustion model. For both power plant models a constant fixed value of coal (as received, 33.93 kg/s), corresponding to a heat input to the plant of 847.9 MW, is assumed as calculation basis, resulting in net power output in the range of 320-400 MW, which are representative values of actual IGCC plants.

4 Results and discussion

4.1 Power Plant performance and Benchmark

In this section, the power breakdown of the different models considered is given. Table 2 shows the results for the pre-combustion capture model and for the two most efficient cases aiming for a high capture rate, which correspond to Steam to GSOP with Selexol treating and Air to Gasifier with MDEA capture; both with a GSOP oxidation temperature of 900 °C.

Table 2: Power breakdown of pre-combustion and OPPC models

Item	OPPC Steam to GSOP	OPPC Air to Gasifier	Pre-combustion Model
CO_2 Capture Technology	Selexol	MDEA	Selective Selexol

Steam Turbine (MW)	160,4	154,1	149.1
Gas Turbine (MW)	262,1	260,0	282.0
Gross Plant (MW)	422,5	414,1	431.1
Net Plant (MW)	384,5	375,5	323.2
LHV Input (MW)	847,9	847,9	847,9
CO_2 Compression & Cooling (MW)	-20,5	-25,0	-26.37
ASU & N_2 compression (MW)	-	-	-59.1
AGRU (MW)	-4,5	-1,0	-11.7
*Other Auxiliaries (MW)	-12,9	-12,5	-10.8
Gross LHV Efficiency (%)	49,8	48,9	50.8
Net LHV Efficiency (%)	45,3	44,3	38.1
Capture Rate (%)	84,3	86,3	90.9
Specific Emissions (kg/MWh)	116,9	104,8	82.9

**Water Pumps, Power Island Auxiliaries, Cooling Duty power, Syngas and fuel recompression, Coal Milling, Ash Handling, Balance of the Plant are considered here.*

OPPC outperforms the conventional pre-combustion capture plant by 7.2 and 6.2 %-points for Steam to GSOP and Air to Gasifier cases respectively. However, this comes at a sacrifice of 6.6 and 4.6 %-points in CO_2 capture ratio in a like for like comparison. The CO_2 emission increase is directly related to the methane formation in the gasifier due to the lack of equilibrium conditions and the mixing originated by the switching of streams in the GSOP reactors. From a net power perspective, an advantage of the OPPC concept is the low auxiliary power consumption compared to the pre-combustion IGCC plant, where a substantial amount of power is dedicated to ASU and N_2 compression. OPPC employing a physical solvent (Selexol) results in a higher efficiency than OPPC with chemical solvent for syngas treating (MDEA) because of the relatively high steam demand for amine regeneration, despite the higher mechanical pumping duty required for Selexol circulation.

The pre-combustion model shows a somewhat optimistic performance compared to results shown in Jansen, Gazzani [30] because of the somewhat higher pressure ratio adopted for the gas turbine. Furthermore, the simplified gas turbine model does not account for cooling flows with detailed heat transfer calculations, with a resulting higher efficiency which becomes smaller at higher combustion temperatures [47]. This work is carried out under the assumption that gas turbines specifically designed for burning hydrogen will be available by the time of deployment. Given that the same TIT of 1360ºC is achieved for all power plant simulations, a fair thermodynamic assessment of the potential of the OPPC configuration relative to the pre-combustion benchmark is still attained.

4.2 Effect of GSOP operating temperature and capture technology

As explained in section 2, OPPC simulations at different GSOP reactor temperatures were done for MDEA and Selexol as absorption technologies. Three temperatures were considered for the GSOP oxidation stage outlet (700, 800 and 900 °C). Figure 7 shows the performance of these models in terms of electrical efficiency and capture rate for the Steam to GSOP and Air to Gasifier cases respectively.

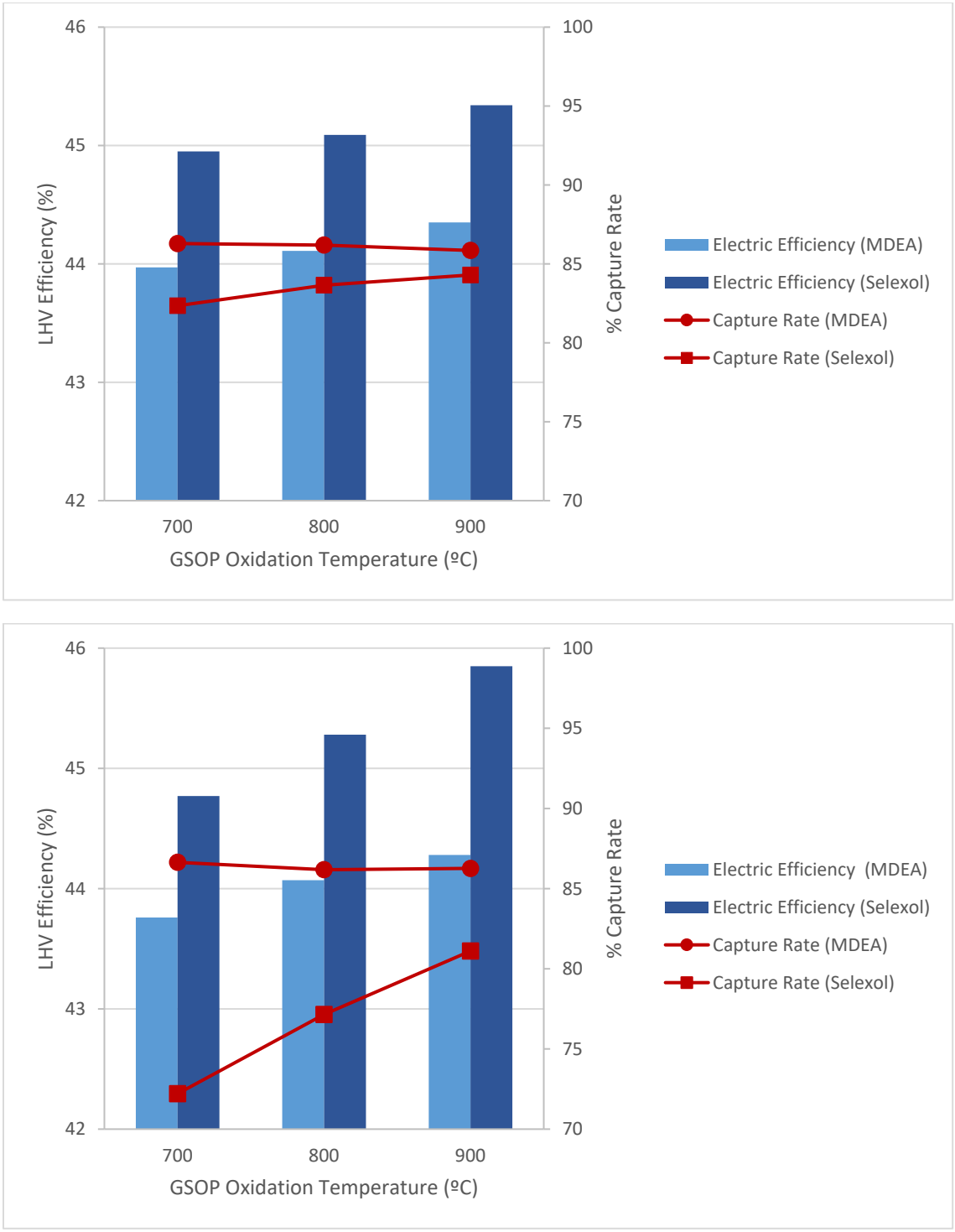

Figure 7: OPPC Steam to GSOP cases (above) and Air to gasifier cases (below) net efficiency and capture rate for different GSOP operating temperatures and capture technologies.

Increasing GSOP temperature has a small positive effect on electrical efficiency. The amount of syngas that is diverted to the GSOP reactors increases with higher oxidation temperatures, as more fuel is required to heat the compressed air to the reactor temperature. Greater preheating of air in the GSOP reactors reduces the amount of hydrogen that needs to be prepared in the pre-combustion section of the plant where significant energy penalties are involved. Avoiding a larger portion of these pre-

combustion capture energy penalties is the primary efficiency-related benefit of higher GSOP temperatures.

As a consequence of the larger sweep gas flowrate at higher GSOP temperatures, the amount of steam from the bottoming cycle added to the sweep gas or the portion of compressed air that is sent to the gasifier is reduced. The higher temperature of the stream sent to the gasifier also reduces the gasifier oxygen demand, further reducing the need for these measures. Figure 8 shows the reduction in steam and N_2 content in the syngas with an increase in GSOP temperature for the Steam to GSOP and Air to Gasifier cases respectively.

Because more CO is being converted in the GSOP, the steam requirements in the WGS section for the Air to gasifier cases decrease, improving the performance of the bottoming cycle. When steam is used to close the energy balance in the gasifier, Figure 8 shows that an increasing GSOP temperature leads to a syngas with a lower H_2/CO ratio (less steam is added to the GSOP reduction stage). This has the drawback of increasing the steam demand in the WGS section to achieve the same CO conversion.

For both cases, more CO_2 is recirculated in the GSOP – Gasifier loop with increasing GSOP oxidation temperature, which leads to an increase of the partial pressure of this component as it enters the WGS. Since CO_2 is a product of the shift reaction, its presence is detrimental to a desired high CO conversion. However, it also absorbs the heat of reaction and reduces the adiabatic temperature rise (improving as a consequence the equilibrium conversion). In the Air to Gasifier cases, N_2 acts as an inert with the same effect, although the relative size of the unit increases when compared to the Steam to GSOP cases, because of the higher volumetric flow rate. Overall, Air to Gasifier cases had on average a CO conversion approximately 1.5% higher than the steam to GSOP cases.

The CO_2 capture penalty when Selexol is employed in the Air to Gasifier cases is more pronounced than for Steam to GSOP cases, since the presence of N_2 leads to a lower partial pressure of CO_2 and consequently the capture performance of the physical solvent is diminished. The lower requirement for additional air to the gasifier at higher GSOP temperatures is the reason for the significant positive effect on Selexol CO_2 capture ratios in the Air to Gasifier case in Figure 7.

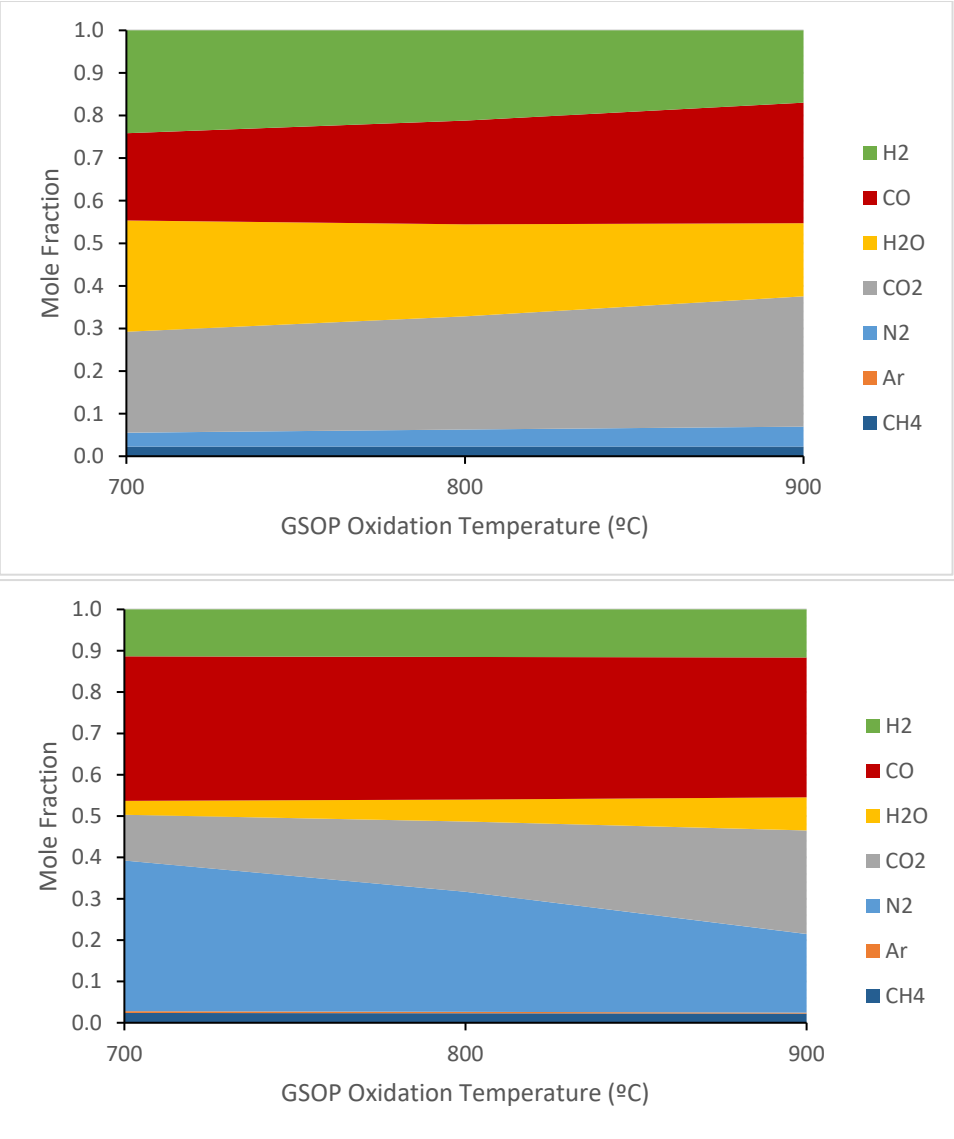

Figure 8: Syngas compositions at different GSOP operating temperature for Steam to GSOP cases (above) and Air to Gasifier cases (below) for the case of MDEA CO_2 removal.

4.3 Plant Emissions Breakdown

It was discussed that a high CO_2 partial pressure increases the attractiveness of a physical absorbent over a chemical absorbent, because of the lower solvent regeneration duty demand of the former. The choice of the absorption technology is not straightforward and this work only attempts to show the trade-off between efficiency and capture rate given the model assumptions and process topology described in section 3. Different design possibilities are available which might favour one technology over the other, such as operating at higher pressure ratios or boosting the syngas pressure before the absorption unit. Methane present in the syngas contributes to a higher cold gas efficiency of the gasifier [48] (higher topping cycle efficiency) but limits the amount of CO_2 that can be captured after the Shift conversion. Its formation is enhanced when the gasifier operates at higher pressures i.e. higher gas turbine pressure ratios (a fixed value was used in the present work because the gasifier operated at the same pressure and temperature in all cases). These items will be subject of study and optimization in future work.

In the present study, a detailed CO_2 emission breakdown has been performed to quantify the different sources of emissions in this plant and their relative weight. Emissions originated from coal loading in

lock hoppers, undesired mixing in GSOP reactor switching stages, methane formation in the gasifier, unconverted CO in the WGS section and CO_2 not absorbed in the treating units are quantified in Figure 9 for both Steam to GSOP and Air to Gasifier cases, based on the capture technology for a GSOP operating temperature of 900 °C. The main source of emissions results from the treating units, followed by the methane formation in the gasifier and GSOP mixing.

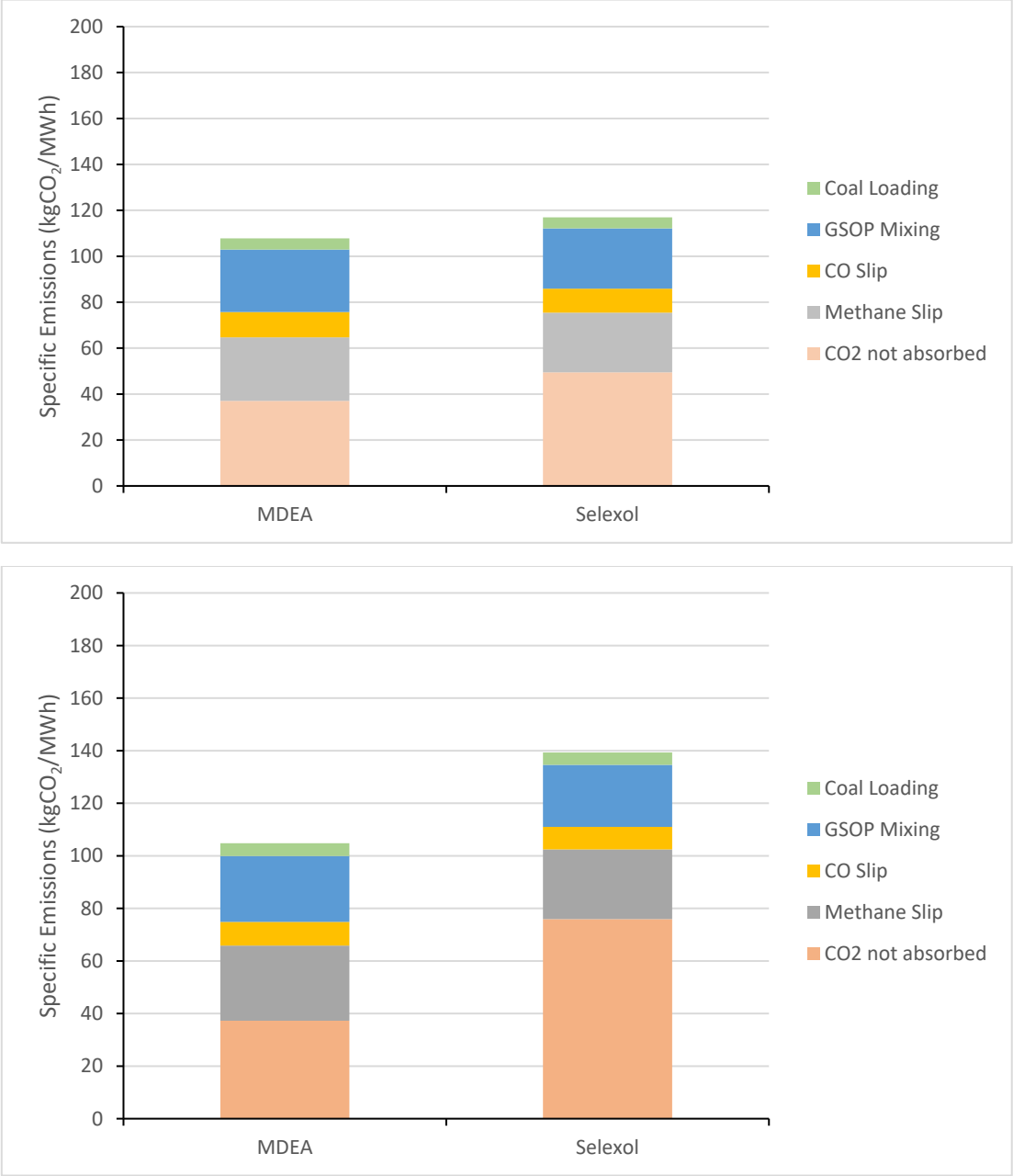

Figure 9: Specific CO_2 emission breakdown for OPPC Steam to GSOP cases (above) and Air to Gasifier cases (below) for GSOP operating temperature of 900ºC.

Figure 10 shows the fraction of emissions that are generated due to undesired stream mixing in the GSOP reactors with varying GSOP oxidation stage operating temperatures. Since the total syngas flowrate to the reactors increases, so does the proportion of emissions in this unit. This is an opportunity to effectively implement, for high GSOP operating temperatures, heat management strategies as described in previous works [23, 49] such as steam purging that would reduce this source of emissions, improving the capture rate of the plant (reaching values close to 90% capture) at the cost

of a slightly lower performance of the bottoming cycle. For the steam to GSOP cases, this would not require further modifications to the plant layout. A reduced mixing scenario for this case will also further limit the small fraction of N_2 in the syngas, reducing recirculation of this component to the Gasifier and increasing the CO_2 partial pressure after Shift, making physical solvents more attractive and efficient.

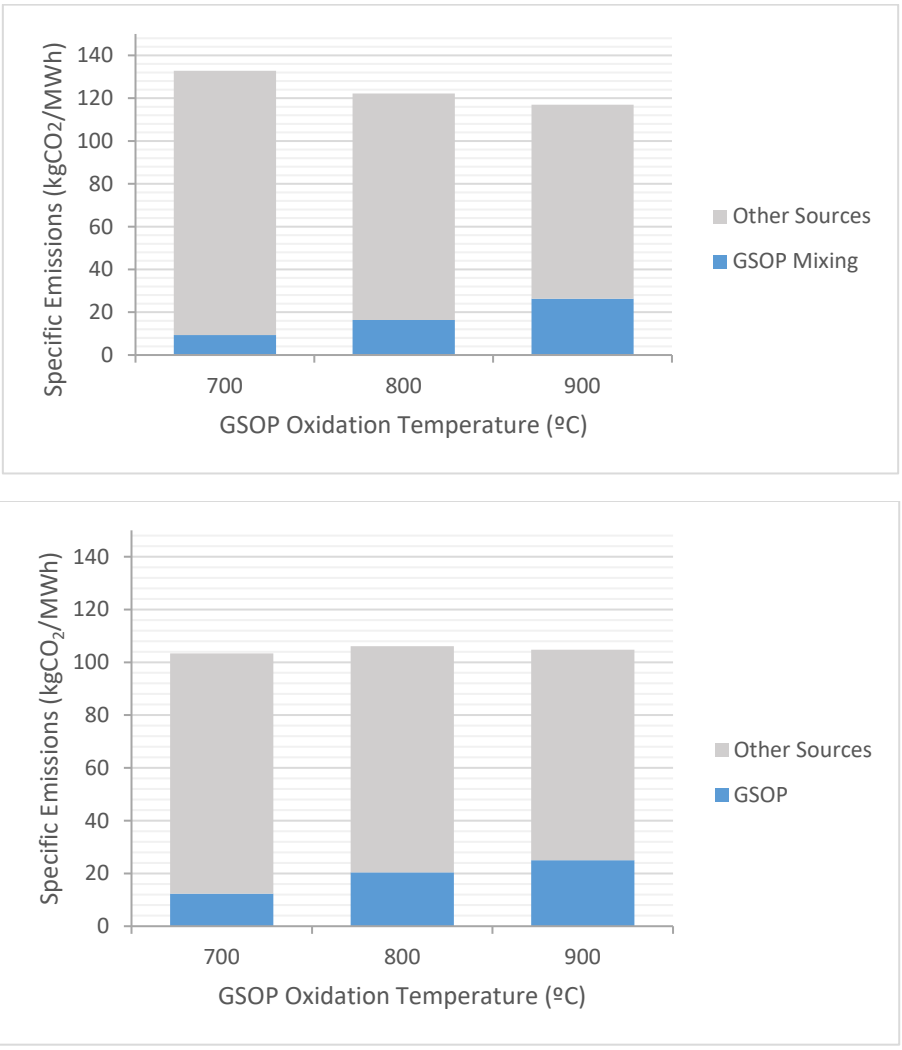

Figure 10: Specific CO_2 emissions for GSOP and overall sources at different GSOP operating temperature for Steam to GSOP case and Selexol treating (above) and Air to Gasifier case with MDEA treating (below).

4.4 Cases with No Syngas Dilution

The steam demand for syngas dilution poses an important energy penalty for the OPPC configurations, since no N_2 from an ASU is available and high grade heat in the WGS section must be used to generate the required steam for dilution. Premixed combustors, extensively used in natural gas combined cycle gas turbines, operate under the principle that more air than stoichiometric can be fed into the combustion zone aiming for a lower flame temperature and consequently lower NOx emissions. In IGCC configurations, with a H_2 rich fuel, diffusion burners with massive syngas dilution are typically employed to circumvent the challenges of air and H_2 mixtures. Several efforts to operate with premixed hydrogen combustors have been studied and a comparison with premixed burners is detailed in Gazzani, Chiesa [50] revealing that avoidance of dilution with premixed combustors can lead to

efficiency gains of around 2%-points with respect to diffusive burners with N_2 fuel dilution and SFT of 2200 K in combined cycle plants.

Since the O_2 depleted air from the GSOP is at a high temperature (900 °C compared to 450 °C in the pre-combustion model), the air being fed to the combustor is significantly above the H_2 autoignition temperature, so it is not required to feed air and fuel close to a stoichiometric ratio to maintain the flame in the combustion zone. If all the air can be fed to the combustion zone, a performance similar to an ideal premixed combustor can be achieved if the degree of fuel-air mixing is maximized by multiple fuel injectors and high turbulence, and it is plausible to achieve low NOx emissions without dilution.

In this work, the effect of dilution avoidance was evaluated for the two OPPC cases presented in Table 1, Steam to GSOP - Selexol treating and Air to Gasifier – MDEA treating with a GSOP oxidation temperature of 900 °C. The same pressure drop in the combustion chamber was considered as for the diluted cases, Figure 11 shows the efficiency improvements obtained. The efficiency gain is primarily due to a higher power output from the bottoming cycle. The gas turbine output is somewhat reduced as a higher flow rate of air must be compressed to achieve the same TIT. The efficiency benefits are lower than Gazzani, Chiesa [50] because of the thermal devaluation due to gasification, syngas treating and H_2 generation from the original fuel in IGCC plants compared to gaseous fuel combined cycles.

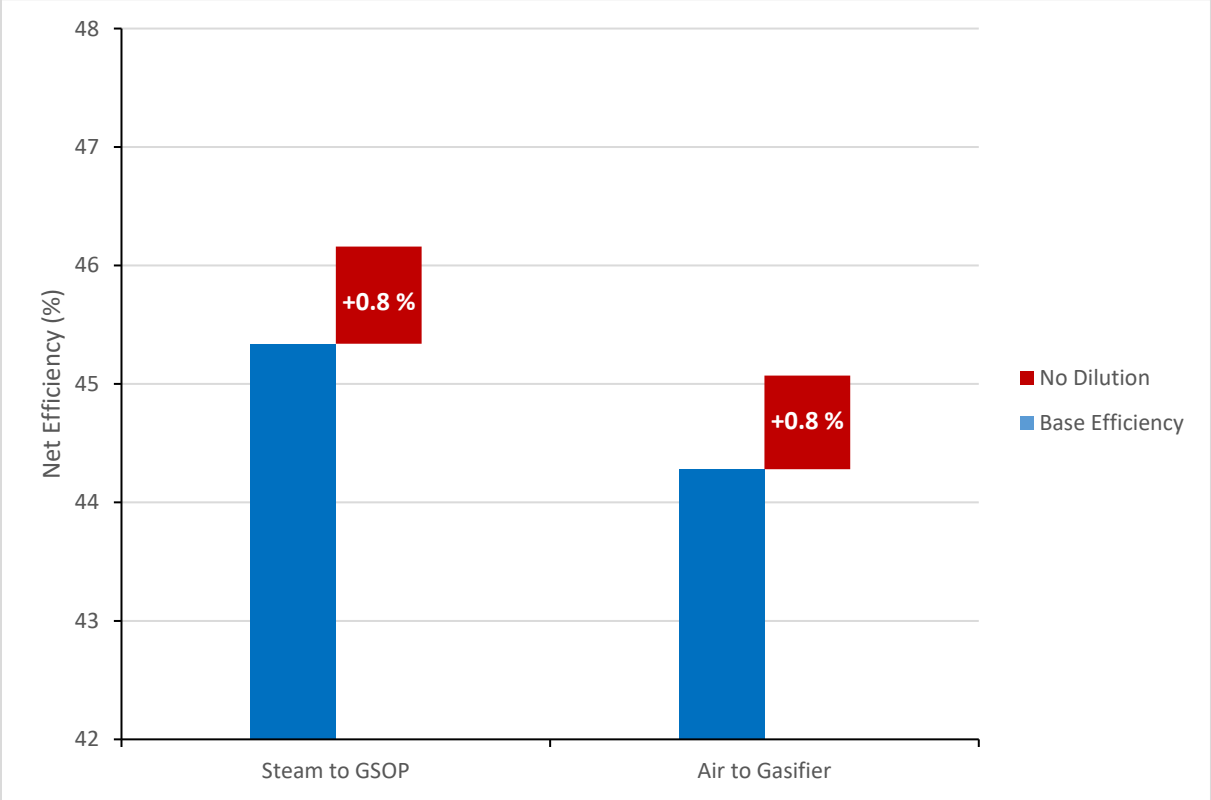

Figure 11: Efficiency improvements for OPPC Steam to GSOP and Air to Gasifier cases with no fuel dilution.

5 Conclusions

In this work, the novel Oxygen Production Pre-Combustion (OPPC) power plant concept was presented. OPPC employs Gas Switching Oxygen Production (GSOP) reactors to achieve around 6 %-points higher efficiency than a conventional pre-combustion CO_2 capture IGCC plant. However, the CO_2 capture ratio was approximately 6 %-points lower, due to the methane formation in the fluidized bed

gasifier of the OPPC plant and undesired mixing of streams in the gas switching reactors. This study has evaluated:

- Two options of closing the gasifier energy balance: employing steam from the bottoming cycle in the GSOP reactor as sweep gas (Steam to GSOP) or diverting a portion of air from the compressor to the oxidizing stream (Air to Gasifier), with similar electric efficiencies.
- Two absorption technologies for CO_2 removal: physical absorption with Selexol over chemical absorption with MDEA yielded approximately 1% point higher efficiencies, but lower capture rates: the configuration employing Steam to GSOP is more suited for physical absorption of CO_2 since in the Air to gasifier cases the presence of incondensable N_2 reduces the CO_2 partial pressure, resulting in lower attainable capture rates.
- A GSOP operating temperature between 700ºC and 900ºC: with increasing efficiencies for higher temperatures. The capture rate performance with Selexol tends to improve for higher GSOP temperatures as the CO_2 partial pressure of the treated syngas increases, while MDEA achieves constant capture performance.

Different options of closing the gasifier energy balance and capturing the CO_2 were investigated, but no clear optimal solution was identified in the trade-off between electric efficiency and CO_2 capture rate. However, results clearly demonstrated that higher GSOP operating temperatures improve both efficiency and CO_2 capture rate.

The fact that the pre-heated air temperature entering the combustor is well above the fuel autoignition temperature will allow lean air-fuel mixtures in the combustion zone, potentially eliminating the need to dilute the fuel with water/steam to avoid NOx formation. This can result in 0.8 %-points of additional efficiency gain. Furthermore, the OPPC plant can benefit from developments in sorption enhanced water gas shift technology [51, 52], to avoid downstream absorption units and the associated auxiliary power demand.

OPPC avoids an important technical concern with previous IGCC plant configurations proposed with gas switching combustion (GSC) technology [23, 28, 35]. These previous works assumed a maximum reactor temperature of 1200 °C (lower values significantly reduce power cycle efficiency [53]), which presents important technical uncertainties related to oxygen carrier material stability, reactor construction materials, as well as downstream valves and filters. Operating GSOP reactors at 900 °C instead of GSC reactors at 1200 °C therefore significantly increases the technical feasibility of gas switching technology for highly efficient power production with CO_2 capture. Plants running on H_2 as fuel such as the OPPC concept can greatly benefit from the increasing development efforts, triggered by decarbonisation policies, that gas turbine manufacturers [54] have undergone in the last years to make heavy-duty industrial turbines with H_2 fuel (above 30%vol) commercially available.

IGCC based processes can become a relevant industrial reality beyond the year 2030 in view of their attractive cost reduction prospects [55] and operational expertise gained in the last decades with demonstration plants. In a scenario of increasingly stringent pollutant regulations and deployment of low carbon footprint technologies, IGCC plants with CCS such as the OPPC plant presented in this work will become a more competitive technology relative to pulverized coal boilers, due to the inherently higher efficiencies and lower environmental impact of other pollutants such as SOx.

5.1 Acknowledgement

The authors gratefully acknowledge the financial support from the ERA-NET cofund, ACT GaSTech Project number 276321 co-funded by the European Commission under the Horizon 2020 program, ACT Grant Agreement No. 691712. The partners collaborating in this article have received funding from

MINECO, Spain (reference PCIN-2017-013) and the Research Council of Norway, Norway. The authors would also like to acknowledge Honeywell for the free Academic License of Unisim Design Suite R451, which enabled integrated GSOP model & power plant simulations.

6 Appendix

Table 3: Shell gasifier island model assumptions.

Air Separation Unit		
Equipment/Item	***Value***	***Units***
Polytropic Efficiency Air Compressor Stage	89	%
Polytropic Efficiency N_2 Compressor Stage	82	%
Reboiler-Condenser Pinch	1.5	ºC
Heat Exchanger Minimum Approach Temperature	2	ºC
Process Stream Temperature after heat rejection	25	ºC
Oxygen Purity	95	%
Oxygen Pressure	48	bar
Oxygen Pump Efficiency	80	%
Exchanger Pressure Losses / side	10	kPa
Intercooler Pressure Loss	10	kPa
Steam for TSA regeneration	58.3	kWh/ton O_2
Gasifier		
Equipment/Item	***Value***	***Units***
Moderator (steam) to dry coal ratio	0.09	kg/kg
Oxygen to dry coal ratio	0.9	kg/kg
Moisture in Coal after drying	2	%
Syngas for coal drying as %LHV	0.9	%
Fixed Carbon Conversion	99.3	%
Gasifier Operating Pressure	44	bar
Steam Moderator Pressure	54	bar
Oxygen to Gasifier Temperature	180	ºC
Heat Loss as %LHV	0.7	%
Heat to Membrane wall as %LHV	2	%
Balance of Plant as %LHV	0.15	%
CO_2 HP/HHP Pressure	56/88	bar
CO_2 Temperature	80	ºC
CO_2 to dry coal ratio	0.83	kg/kg
Coal Milling & Handling	100	kJ/kg coal
Ash Handling	50	kJ/kg ash
Syngas Quench & Convective Cooler		
Equipment/Item	***Value***	***Units***
Quenched Syngas Temperature	900	ºC
Cold Recycle Gas Temperature	300	ºC
Recycle Fan Polytropic Efficiency	80	%
Recycle Fan Mechanical Efficiency	95	%
Syngas Effluent Cooler Pressure Drop	4	%
Syngas Effluent Cooler Heat Loss	0.7	%
Superheat Steam Temperature in SEC	450	ºC

Table 4: High temperature Winkler gasifier island assumptions

Gasifier		
Equipment/Item	***Value***	***Units***
Gasifier Freeboard Temperature	900	ºC
Fixed Carbon Conversion	97	%
Heat Loss as % LHV	0.5	%
LHV Methane in Syngas / LHV Input	11.3	%
Gasifier Pressure	19.3	bar
CO_2 for coal loading	0.15	kg CO_2/ kg coal
CO_2 Conditions	42/80	bar/ºC
CO_2 vented in Lock Hoppers	10	%
Balance of Plant as % LHV	0.15	%
Coal Milling	40	kJe/kg coal
Ash Handling	200	kJe/kg ash
Convective Cooler		
Equipment/Item	***Value***	***Units***
Syngas Outlet Temperature	400	ºC
Syngas Pressure Drop	50	kPa
Steam Superheat	450	ºC
Heat Loss	0.7	%

Table 5: Syngas treating modelling assumptions.

Hot Gas Clean Up		
Equipment/Item	***Value***	***Units***
Syngas Temperature at Adsorption Bed	400	ºC
Electric Consumption of Auxiliaries	5.34	MJ_e/kg H_2S
Gas Filter Pressure Loss	5	%
Desorption Compander Duty	1.8	kWs / kg syngas

Table 6: Water gas shift modelling assumptions.

Water Gas Shift		
Equipment/Item	***Value***	***Units***
Nº of reactors	2	-
HTS Inlet Temperature	250	ºC
LTS Temperature	200	ºC
Steam to CO ratio	1.9	-
Heat Losses	0.8	%
Multistream Heat Exchanger Pinch	10	ºC
Syngas Side Total Pressure Loss	1.8	bar

Table 7: GSOP & firing chamber modelling assumptions.

GSOP & Firing Chamber		
Equipment/Item	***Value***	***Units***
GSOP Reactor Pressure Drop	4	%
Combustor Pressure Drop / Precombustion IGCC	30/50	kPa
Combustor Outlet Temperature	1360	ºC
Fuel Temperature at Combustor Inlet	180	ºC

Table 8: Absorption units modelling assumptions.

Selexol		
Equipment/Item	***Value***	***Units***
Absorber Temperature	25	ºC
% Syngas to H_2S Concentrator	20	%
% mol H_2S to Claus Unit	>25	%
H_2S in CO_2 compressed	<20	ppm
Recycle Compressors Isentropic Efficiency	80	%
Lean – H_2S laden solvent Exchanger pinch	5	ºC
Pressure Levels HP/MP/LP	6/2.5/1	bar
Solvent Pump Isentropic Efficiency	80	%
MDEA		
Equipment/Item	***Value***	***Units***
Lean Amine Loading	1	%
Equilibrium Stages	12	-
Stage Efficiency	35	%
Amine Exchanger Pinch	5	ºC
Absorber Pressure Drop	0.5	bar
Stripper Pressure	1.25	bar
Solvent %w. MDEA	50	%
Solvent Pump Isentropic Efficiency	80	%

Table 9: CO_2 compression & auxiliary compression.

CO_2, Syngas & Fuel Compressor		
Equipment/Item	***Value***	***Units***
Nº of Compressor stages	5	-
Intercooler Outlet Temperature	25	ºC
Intercooler Pressure Drop / stage	5/10/20/40/80	kPa
Compressor Stage Isentropic Efficiency	80	%
CO_2 Pump Isentropic Efficiency	80	%
Syngas Recompression Polytropic Efficiency	80	%
Fuel Compressor Polytropic Efficiency	80	%
Mechanical Efficiency	95	%

Table 10: Power plant feedstock characteristics.

Coal: Douglas Premium	
Element	% weight
C	66.52
H	3.78
O	5.46
N	1.56
S	0.52
Moisture	8.00
Ash	14.15
Thermal Properties	
LHV (MJ/kg)	24.99
HHV (MJ/kg)	25.80

Table 11: Power island modelling assumptions.

Gas Turbine		
Equipment/Item	***Value***	***Units***
Air Compressor Polytropic Efficiency	90	%
Gas Turbine Isentropic Efficiency	92	%
Pressure Ratio	20	-
Air Filter Pressure Loss	1	%
Air Compressor Leakage	0.75	% inlet flow
Gas Turbine Auxiliary Consumption	0.35	% net power
Gas Turbine Mechanical Efficiency	99.86	%
Generator Efficiency	98.7	%
Steam Turbine		
Equipment/Item	***Value***	***Units***
Steam HP/IP/LP Stage Isentropic Efficiency	92/94/88	%
Condensing Pressure	0.048	bar
Turbine Mechanical Efficiency	99.6	%
Generator Efficiency	98.5	%
Water Pumps Adiabatic Efficiency	80	%
Power for Heat Rejection	0.008	MJe/MJth
Heat Recovery Steam Generators		
Equipment/Item	***Value***	***Units***
HP/IP/LP Pressure Levels	144/36/4	bar
Gas-Gas Temperature Minimum Approach	20	ºC
Pinch Point	10	ºC
Approach Point	5	ºC
Maximum SH/RH Steam Temperature	565	ºC
Minimum Stack Outlet Temperature	100	ºC
Economizer Pressure Loss	1	%
Evaporator Pressure Loss	4	%
Superheater Pressure Loss	3	%
HRSG Air Pressure Loss	3	kPa
HRSG Heat Loss	0.7	% heat transferred

Table 12: Stream data for pre-combustion model.

Property					*Composition (%)*								
Steam	Mass Flow (kg/s)	MW (kg/kmol)	P (bar)	T (ºC)	N_2	O_2	Ar	CO	CO_2	CH_4	H_2	H_2O	H_2S
1	31,85	Dry Douglas Premium Coal											
2	123,9	22,9	44,0	900,1	0,94	0,00	1,19	62,27	7,10	0,13	22,37	5,81	0,18
3	126,5	23,1	42,0	295,8	0,94	0,00	1,19	62,27	7,10	0,13	22,37	5,81	0,18
4	58,6	23,0	44,0	288,0	0,92	0,00	1,16	60,61	7,99	0,13	21,77	7,25	0,17
5	128,2	20,4	41,0	260,5	0,44	0,00	0,56	29,15	3,84	0,06	10,47	55,40	0,08
6	128,2	20,4	38,0	247,0	0,44	0,00	0,56	0,52	32,47	0,06	39,10	26,77	0,08
7	11,4	4,4	36,0	36,0	1,05	0,00	1,30	1,23	3,07	0,14	93,18	0,03	0,00
8	77,3	15,0	25,0	24,0	39,22	0,00	0,69	0,62	1,55	0,07	46,97	10,88	0,00
9	397,0	28,9	1,0	15,0	77,30	0,00	0,92	0,00	0,04	0,00	0,00	1,01	0,00
10	394,1	28,9	20,1	447,3	77,30	0,00	0,92	0,00	0,04	0,00	0,00	1,01	0,00
11	471,3	26,8	19,5	1360,0	71,54	9,11	0,91	0,00	0,68	0,00	0,00	17,75	0,00
12	471,3	26,8	1,0	615,9	71,54	9,11	0,91	0,00	0,68	0,00	0,00	17,75	0,00
13	471,3	26,8	1,0	118,0	71,54	9,11	0,91	0,00	0,68	0,00	0,00	17,75	0,00
14	117,8	26,8	1,0	15,0	71,54	9,11	0,91	0,00	0,68	0,00	0,00	17,75	0,00
15	28,8	32,3	48,0	180,0	1,10	94,99	3,91	0,00	0,00	0,00	0,00	0,00	0,00
16	55,8	28,0	24,0	152,6	99,91	0,00	0,09	0,00	0,00	0,00	0,00	0,00	0,00
17	130,0	18,0	144,0	565,0	0,00	0,00	0,00	0,00	0,00	0,00	0,00	100,00	0,00
18	87,3	18,0	40,0	565,0	0,00	0,00	0,00	0,00	0,00	0,00	0,00	100,00	0,00
19	80,0	18,0	155,6	61,7	0,00	0,00	0,00	0,00	0,00	0,00	0,00	100,00	0,00
20	63,6	18,0	148,5	450,0	0,00	0,00	0,00	0,00	0,00	0,00	0,00	100,00	0,00
21	52,9	18,0	41,2	363,3	0,00	0,00	0,00	0,00	0,00	0,00	0,00	100,00	0,00
22	7,0	18,0	6,5	292,0	0,00	0,00	0,00	0,00	0,00	0,00	0,00	100,00	0,00
23	76,8	18,0	0,0	32,2	0,00	0,00	0,00	0,00	0,00	0,00	0,00	100,00	0,00
24	74,1	43,8	150,0	25,0	0,01	0,00	0,05	0,02	99,38	0,01	0,37	0,17	0,00
25	26,3	43,8	54/88	80,0	0,01	0,00	0,05	0,02	99,38	0,01	0,37	0,17	0,00

Table 13: Stream data for OPPC Air to Gasifier case with GSOP oxidation temperature of 900ºC and MDEA treating.

Property					*Composition (% mol)*								
Steam	m (kg/s)	MW (kg/kmol)	P (bar)	T (ºC)	N_2	O_2	Ar	CO	CO_2	CH_4	H_2	H_2O	H_2S
1	33,93	Douglas Premium Coal											
2	146,80	27,95	19,26	900,00	19,01	0,00	0,22	33,79	24,99	2,22	11,62	8,04	0,10
3	146,80	27,95	18,76	400,00	19,01	0,00	0,22	33,79	24,99	2,22	11,62	8,04	0,10
4	61,53	27,95	20,06	423,20	19,04	0,00	0,22	33,82	25,04	2,22	11,64	8,01	0,00
5	85,03	27,95	17,82	399,90	19,04	0,00	0,22	33,82	25,04	2,22	11,64	8,01	0,00
6	30,82	18,02	36,00	245,10	0,00	0,00	0,00	0,00	0,00	0,00	0,00	100,00	0,00
7	115,90	24,38	17,32	436,30	12,19	0,00	0,14	3,60	34,07	1,42	25,49	23,08	0,00
8	115,90	24,38	16,62	233,70	12,19	0,00	0,14	0,45	37,23	1,42	28,65	19,93	0,00
9	24,81	11,68	19,76	45,61	27,26	0,00	0,32	1,01	4,16	3,18	64,08	0,00	0,00
10	41,18	13,57	19,66	180,00	19,09	0,00	0,22	0,70	2,91	2,23	44,88	29,96	0,00
11	547,60	28,85	1,01	15,00	77,30	20,73	0,92	0,00	0,04	0,00	0,00	0,00	1,01
12	543,50	28,85	20,06	447,30	77,30	20,73	0,92	0,00	0,04	0,00	0,00	0,00	1,01
13	490,90	28,69	19,26	899,00	81,82	15,61	0,98	0,00	0,39	0,00	0,00	1,21	0,00
14	532,10	27,36	18,96	1360,00	76,74	11,09	1,31	0,00	2,01	0,00	0,00	8,85	0,00
15	532,10	27,36	1,04	615,70	76,74	11,09	1,31	0,00	2,01	0,00	0,00	8,85	0,00
16	532,10	27,36	1,01	100,50	76,74	11,09	1,31	0,00	2,01	0,00	0,00	8,85	0,00
17	114,10	33,30	19,26	854,10	24,06	17,83	0,41	0,00	49,58	0,00	0,00	8,12	0,00
AtG	17,80	28,85	20,06	447,30	77,30	20,73	0,92	0,00	0,04	0,00	0,00	0,00	1,01
18	63,61	18,02	146,50	450,00	0,00	0,00	0,00	0,00	0,00	0,00	0,00	100,00	0,00
19	104,50	18,02	144,00	565,00	0,00	0,00	0,00	0,00	0,00	0,00	0,00	100,00	0,00
20	104,50	18,02	36,00	565,00	0,00	0,00	0,00	0,00	0,00	0,00	0,00	100,00	0,00
21	72,70	18,02	0,05	32,17	0,00	0,00	0,00	0,00	0,00	0,00	0,00	100,00	0,00
22	22,20	18,02	39,05	32,27	0,00	0,00	0,00	0,00	0,00	0,00	0,00	100,00	0,00
23	34,82	18,02	1,80	174,30	0,00	0,00	0,00	0,00	0,00	0,00	0,00	100,00	0,00
24	5,09	43,94	41,90	50,00	0,00	0,00	0,00	0,00	99,74	0,00	0,00	0,26	0,00
25	68,69	43,94	150,00	35,00	0,00	0,00	0,00	0,00	99,74	0,00	0,00	0,26	0,00

Table 14: Stream data for OPPC model Steam to GSOP case with GSOP operating temperature of 900ºC and Selexol treating.

Property					*Composition (% mol)*								
Steam	Mass Flow (kg/s)	MW (kg/kmol)	P (bar)	T (ºC)	N_2	O_2	Ar	CO	CO_2	CH_4	H_2	H_2O	H_2S
1	33,93	Douglas Premium Coal											
2	143,30	26,46	19,26	900,00	4,72	0,00	0,05	28,20	30,41	2,17	17,09	17,25	0,10
3	143,30	26,46	18,76	400,00	4,72	0,00	0,05	28,20	30,41	2,17	17,09	17,25	0,10
4	62,51	26,45	20,06	422,30	4,73	0,00	0,05	28,23	30,44	2,18	17,11	17,27	0,00
5	80,62	26,45	17,82	399,90	4,73	0,00	0,05	28,23	30,44	2,18	17,11	17,27	0,00
6	20,08	18,02	36,56	245,50	0,00	0,00	0,00	0,00	0,00	0,00	0,00	100,00	0,00
7	100,70	24,19	17,32	418,60	3,46	0,00	0,04	4,07	38,89	1,59	29,13	22,82	0,00
8	100,70	24,19	16,62	236,20	3,46	0,00	0,04	0,62	42,34	1,59	32,57	19,28	0,00
9	13,79	8,11	19,76	45,97	8,37	0,00	0,08	1,49	7,06	3,70	79,23	0,07	0,00
10	33,33	11,96	19,66	180,00	5,11	0,00	0,05	0,91	4,31	2,26	48,38	38,98	0,00
11	537,40	28,85	1,01	15,00	77,30	20,73	0,92	0,00	0,04	0,00	0,00	0,00	1,01
12	533,40	28,85	20,06	447,30	77,30	20,73	0,92	0,00	0,04	0,00	0,00	0,00	1,01
13	494,00	28,65	19,26	900,00	82,13	15,04	0,98	0,00	0,41	0,00	0,00	1,43	0,00
14	527,30	27,26	18,96	1360,00	75,98	10,80	1,29	0,00	2,33	0,00	0,00	9,59	0,00
15	527,30	27,26	1,04	617,30	75,98	10,80	1,29	0,00	2,33	0,00	0,00	9,59	0,00
16	527,30	27,26	1,01	100,40	75,98	10,80	1,29	0,00	2,33	0,00	0,00	9,59	0,00
17	110,70	31,09	19,26	915,30	6,68	16,88	0,08	0,00	38,60	0,00	0,00	37,76	0,00
StG	8,82	18,02	36,00	565,00	0,00	0,00	0,00	0,00	0,00	0,00	0,00	100,00	0,00
18	68,69	18,02	146,50	565,00	0,00	0,00	0,00	0,00	0,00	0,00	0,00	100,00	0,00
19	108,30	18,02	144,00	565,00	0,00	0,00	0,00	0,00	0,00	0,00	0,00	100,00	0,00
20	95,20	18,02	36,00	565,00	0,00	0,00	0,00	0,00	0,00	0,00	0,00	100,00	0,00
21	98,70	18,02	0,05	32,17	0,00	0,00	0,00	0,00	0,00	0,00	0,00	100,00	0,00
22	14,76	18,02	39,05	32,27	0,00	0,00	0,00	0,00	0,00	0,00	0,00	100,00	0,00
23	0.00	-											
24	5,09	43,69	42,00	50,00	0,10	0,00	0,00	0,04	99,02	0,20	0,47	0,17	0,00
25	67,23	43,69	150,00	35,00	0,10	0,00	0,00	0,04	99,02	0,20	0,47	0,17	0,00

7 References

[1] IPCC. Global Warming of 1.5 °C. Intergovernmental Panel on Climate Change2018.
[2] B. He, C. Chen. Energy ecological efficiency of coal fired plant in China. Energy Conversion and Management. 43 (2002) 2553-67.
[3] K. Kanellopoulos. Scenario analysis of accelerated coal phase-out by 2030: A study on the European power system based on the EUCO27 scenario using the METIS model. Publications Office of the European Union2018.
[4] M.D. Leonard, E.E. Michaelides, D.N. Michaelides. Substitution of coal power plants with renewable energy sources – Shift of the power demand and energy storage. Energy Conversion and Management. 164 (2018) 27-35.
[5] B. Lin, X. Ouyang. Energy demand in China: Comparison of characteristics between the US and China in rapid urbanization stage. Energy Conversion and Management. 79 (2014) 128-39.
[6] IPCC. Fifth assessment report: Mitigation of climate change. Intergovernmental panel on Climate Change2014.
[7] E.S. Rubin, J.E. Davison, H.J. Herzog. The cost of CO2 capture and storage. International Journal of Greenhouse Gas Control. 40 (2015) 378-400.
[8] J. Marx, A. Schreiber, P. Zapp, M. Haines, J.F. Hake, J. Gale. Environmental evaluation of CCS using Life Cycle Assessment–A synthesis report. Energy Procedia. 4 (2011) 2448-56.
[9] M. Ishida, D. Zheng, T. Akehata. Evaluation of a chemical-looping-combustion power-generation system by graphic exergy analysis. Energy. 12 (1987) 147-54.
[10] A. Lyngfelt, B. Leckner, T. Mattisson. A fluidized-bed combustion process with inherent CO2 separation; Application of chemical-looping combustion. Chem Eng Sci. 56 (2001) 3101-13.
[11] A. Lyngfelt, B. Leckner. A 1000 MWth boiler for chemical-looping combustion of solid fuels – Discussion of design and costs. Applied Energy. 157 (2015) 475-87.
[12] A. Lyngfelt. Chemical-looping combustion of solid fuels – Status of development. Applied Energy. 113 (2014) 1869-73.
[13] A. Abad, J. Adánez, P. Gayán, L.F. de Diego, F. García-Labiano, G. Sprachmann. Conceptual design of a 100 MWth CLC unit for solid fuel combustion. Applied Energy. 157 (2015) 462-74.
[14] T. Mattisson, M. Keller, C. Linderholm, P. Moldenhauer, M. Rydén, H. Leion, et al. Chemical-looping technologies using circulating fluidized bed systems: Status of development. Fuel Processing Technology. 172 (2018) 1-12.
[15] F. Zerobin, T. Pröll. Potential and limitations of power generation via chemical looping combustion of gaseous fuels. International Journal of Greenhouse Gas Control. 64 (2017) 174-82.
[16] R. Naqvi, O. Bolland. Multi-stage chemical looping combustion (CLC) for combined cycles with CO2 capture. International Journal of Greenhouse Gas Control. 1 (2007) 19-30.
[17] F. Petrakopoulou, A. Boyano, M. Cabrera, G. Tsatsaronis. Exergoeconomic and exergoenvironmental analyses of a combined cycle power plant with chemical looping technology. International Journal of Greenhouse Gas Control. 5 (2011) 475-82.
[18] B. Hassan, O.V. Ogidiama, M.N. Khan, T. Shamim. Energy and Exergy Analyses of a Power Plant With Carbon Dioxide Capture Using Multistage Chemical Looping Combustion. Journal of Energy Resources Technology. 139 (2016) 032002--9.
[19] Á. Jiménez Álvaro, I. López Paniagua, C. González Fernández, J. Rodríguez Martín, R. Nieto Carlier. Simulation of an integrated gasification combined cycle with chemical-looping combustion and carbon dioxide sequestration. Energy Conversion and Management. 104 (2015) 170-9.
[20] H. Shijaz, Y. Attada, V.S. Patnaikuni, R. Vooradi, S.B. Anne. Analysis of integrated gasification combined cycle power plant incorporating chemical looping combustion for environment-friendly utilization of Indian coal. Energy Conversion and Management. 151 (2017) 414-25.
[21] E. Ito, K. Tsukagoshi, J. Masada, K. Ishazaka, K. Saitoh, T. Torigoe. Key Technologies for Ultra-High Temperature Gas Turbines. Mitsubishi Heavy Industries Technical Review. 52 (2015).

[22] A. Zaabout, S. Cloete, S.T. Johansen, M. van Sint Annaland, F. Gallucci, S. Amini. Experimental Demonstration of a Novel Gas Switching Combustion Reactor for Power Production with Integrated CO2 Capture. Industrial & Engineering Chemistry Research. 52 (2013) 14241-50.
[23] S. Cloete, M.C. Romano, P. Chiesa, G. Lozza, S. Amini. Integration of a Gas Switching Combustion (GSC) system in integrated gasification combined cycles. International Journal of Greenhouse Gas Control. 42 (2015) 340-56.
[24] B. Moghtaderi. Application of Chemical Looping Concept for Air Separation at High Temperatures. Energy & Fuels. 24 (2010) 190-8.
[25] Z. Deng, B. Jin, Y. Zhao, H. Gao, Y. Huang, X. Luo, et al. Process simulation and thermodynamic evaluation for chemical looping air separation using fluidized bed reactors. Energy Conversion and Management. 160 (2018) 289-301.
[26] K. Wang, Q. Yu, L. Hou, Z. Zuo, Q. Qin, H. Ren. Simulation and energy consumption analysis of chemical looping air separation system on Aspen Plus. Journal of Thermal Analysis and Calorimetry. 124 (2016) 1555-60.
[27] B. Shi, E. Wu, W. Wu. Novel design of chemical looping air separation process for generating electricity and oxygen. Energy. 134 (2017) 449-57.
[28] S. Cloete, A. Giuffrida, M. Romano, P. Chiesa, M. Pishahang, Y. Larring. Integration of chemical looping oxygen production and chemical looping combustion in integrated gasification combined cycles. Fuel. 220 (2018) 725-43.
[29] S. Cloete, A. Tobiesen, J. Morud, M. Romano, P. Chiesa, A. Giuffrida, et al. Economic assessment of chemical looping oxygen production and chemical looping combustion in integrated gasification combined cycles. International Journal of Greenhouse Gas Control. 78 (2018) 354-63.
[30] D. Jansen, M. Gazzani, G. Manzolini, E.v. Dijk, M. Carbo. Pre-combustion CO2 capture. International Journal of Greenhouse Gas Control. 40 (2015) 167-87.
[31] T. Motohashi, Y. Hirano, Y. Masubuchi, K. Oshima, T. Setoyama, S. Kikkawa. Oxygen Storage Capability of Brownmillerite-type Ca2AlMnO5+δ and Its Application to Oxygen Enrichment. Chemistry of Materials. 25 (2013) 372-7.
[32] R.H. Görke, W. Hu, M.T. Dunstan, J.S. Dennis, S.A. Scott. Exploration of the material property space for chemical looping air separation applied to carbon capture and storage. Applied Energy. 212 (2018) 478-88.
[33] Z. Kapetaki, P. Brandani, S. Brandani, H. Ahn. Process simulation of a dual-stage Selexol process for 95% carbon capture efficiency at an integrated gasification combined cycle power plant. International Journal of Greenhouse Gas Control. 39 (2015) 17-26.
[34] D. Jones, D. Bhattacharyya, R. Turton, S.E. Zitney. Optimal design and integration of an air separation unit (ASU) for an integrated gasification combined cycle (IGCC) power plant with CO2 capture. Fuel Processing Technology. 92 (2011) 1685-95.
[35] V. Spallina, M.C. Romano, P. Chiesa, F. Gallucci, M. van Sint Annaland, G. Lozza. Integration of coal gasification and packed bed CLC for high efficiency and near-zero emission power generation. International Journal of Greenhouse Gas Control. 27 (2014) 28-41.
[36] G. Manzolini, E. Macchi, M. Gazzani. CO2 capture in Integrated Gasification Combined Cycle with SEWGS – Part B: Economic assessment. Fuel. 105 (2013) 220-7.
[37] E. Martelli, T. Kreutz, M. Carbo, S. Consonni, D. Jansen. Shell coal IGCCS with carbon capture: Conventional gas quench vs. innovative configurations. Applied Energy. 88 (2011) 3978-89.
[38] F. Franco, R. Anantharaman, O. Bolland, N. Booth, E. van Dorst, C. Ekstrom, et al. European Best Practice Guidelines for CO2 Capture Technologies. CESAR project: European Seventh Framework Programme2011.
[39] R.-Y. Chein, C.-T. Yu. Thermodynamic equilibrium analysis of water-gas shift reaction using syngases-effect of CO2 and H2S contents. Energy. 141 (2017) 1004-18.
[40] P. Chiesa, G. Lozza, L. Mazzocchi. Using Hydrogen as Gas Turbine Fuel. Journal of Engineering for Gas Turbines and Power. 127 (2005) 73-80.
[41] S. Heidenreich. Hot gas filtration – A review. Fuel. 104 (2013) 83-94.

[42] D. Toporov, R. Abraham. Gasification of low-rank coal in the High-Temperature Winkler (HTW) process. Journal of the Southern African Institute of Mining and Metallurgy. 115 (2015) 589-97.
[43] C. Higman, M. van der Burgt. Gasification, 2nd Edition. Gulf Professional Publishing2008.
[44] Y. Ohtsuka, N. Tsubouchi, T. Kikuchi, H. Hashimoto. Recent progress in Japan on hot gas cleanup of hydrogen chloride, hydrogen sulfide and ammonia in coal-derived fuel gas. Powder Technology. 190 (2009) 340-7.
[45] S. Moioli, A. Giuffrida, M.C. Romano, L.A. Pellegrini, G. Lozza. Assessment of MDEA absorption process for sequential H2S removal and CO2 capture in air-blown IGCC plants. Applied Energy. 83 (2016) 1452-70.
[46] M.C. Romano, P. Chiesa, G. Lozza. Pre-combustion CO2 capture from natural gas power plants, with ATR and MDEA processes. International Journal of Greenhouse Gas Control. 4 (2010) 785-97.
[47] J.H. Horlock. Chapter 4 - CYCLE EFFICIENCY WITH TURBINE COOLING (COOLING FLOW RATES SPECIFIED). in: J.H. Horlock, (Ed.). Advanced Gas Turbine Cycles. Pergamon, Oxford, 2003. pp. 47-69.
[48] N. Holt. Gasification Process Selection- Trade-offs and Ironies. Gasification Technologies Conference2004.
[49] S. Cloete, A. Zaabout, M.C. Romano, P. Chiesa, G. Lozza, F. Gallucci, et al. Optimization of a Gas Switching Combustion process through advanced heat management strategies. Applied Energy. 185, Part 2 (2017) 1459-70.
[50] M. Gazzani, P. Chiesa, E. Martelli, S. Sigali, I. Brunetti. Using Hydrogen as Gas Turbine Fuel: Premixed Versus Diffusive Flame Combustors. Journal of Engineering for Gas Turbines and Power. 136 (2014) 051504--10.
[51] H. Lu, Y. Lu, M. Rostam-Abadi. CO2 sorbents for a sorption-enhanced water–gas-shift process in IGCC plants: A thermodynamic analysis and process simulation study. International Journal of Hydrogen Energy. 38 (2013) 6663-72.
[52] M. Gazzani, E. Macchi, G. Manzolini. CO2 capture in integrated gasification combined cycle with SEWGS – Part A: Thermodynamic performances. Fuel. 105 (2013) 206-19.
[53] C. Arnaiz del Pozo, S. Cloete, J.H. Cloete, Á. Jiménez Álvaro, S. Amini. The potential of chemical looping combustion using the gas switching concept to eliminate the energy penalty of CO2 capture. International Journal of Greenhouse Gas Control. 83 (2019) 265-81.
[54] K. Kawai. Hydrogen power generation handbook. Mitsubishi Hitachi Power Systems.
[55] IEA. Projected Costs of Generating Electricity. International Energy Agency and Nuclear Energy Agency2015.